NASA/TM–2015–218934

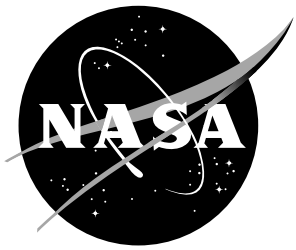

Design and characterization of a new nozzle in a NASA arc-jet

Dinesh K. Prabhu
AMA, Inc. at NASA Ames Research Center, Moffett Field, CA

Imelda Terrazas-Salinas
NASA Ames Research Center, Moffett Field, CA

Eric A. Noyes
Jacobs Technology at NASA Ames Research Center, Moffett Field, CA

John A. Balboni
NASA Ames Research Center, Moffett Field, CA

November 2015

NASA STI Program ... in Profile

Since its founding, NASA has been dedicated to the advancement of aeronautics and space science. The NASA scientific and technical information (STI) program plays a key part in helping NASA maintain this important role.

The NASA STI Program operates under the auspices of the Agency Chief Information Officer. It collects, organizes, provides for archiving, and disseminates NASA's STI. The NASA STI Program provides access to the NASA Aeronautics and Space Database and its public interface, the NASA Technical Report Server, thus providing one of the largest collection of aeronautical and space science STI in the world. Results are published in both non-NASA channels and by NASA in the NASA STI Report Series, which includes the following report types:

- TECHNICAL PUBLICATION. Reports of completed research or a major significant phase of research that present the results of NASA programs and include extensive data or theoretical analysis. Includes compilations of significant scientific and technical data and information deemed to be of continuing reference value. NASA counterpart of peer-reviewed formal professional papers, but having less stringent limitations on manuscript length and extent of graphic presentations.
- TECHNICAL MEMORANDUM. Scientific and technical findings that are preliminary or of specialized interest, e.g., quick release reports, working papers, and bibliographies that contain minimal annotation. Does not contain extensive analysis.
- CONTRACTOR REPORT. Scientific and technical findings by NASA-sponsored contractors and grantees.
- CONFERENCE PUBLICATION. Collected papers from scientific and technical conferences, symposia, seminars, or other meetings sponsored or co-sponsored by NASA.
- SPECIAL PUBLICATION. Scientific, technical, or historical information from NASA programs, projects, and missions, often concerned with subjects having substantial public interest.
- TECHNICAL TRANSLATION. English-language translations of foreign scientific and technical material pertinent to NASA's mission.

Specialized services also include organizing and publishing research results, distributing specialized research announcements and feeds, providing information desk and personal search support, and enabling data exchange services.

For more information about the NASA STI Program, see the following:

- Access the NASA STI program home page at ***http://www.sti.nasa.gov***
- E-mail your question to help@sti.nasa.gov
- Fax your question to the NASA STI Information Desk at 443-757-5803
- Phone the NASA STI Information Desk at 443-757-5802
- Write to:
  NASA STI Information Desk
  NASA Center for AeroSpace Information
  7115 Standard Drive
  Hanover, MD 21076–1320

NASA/TM–2015–218934

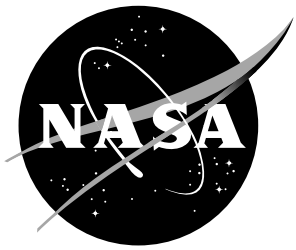

Design and characterization of a new nozzle in a NASA arc-jet

Dinesh K. Prabhu
AMA, Inc. at NASA Ames Research Center, Moffett Field, CA

Imelda Terrazas-Salinas
NASA Ames Research Center, Moffett Field, CA

Eric A. Noyes
Jacobs Technology at NASA Ames Research Center, Moffett Field, CA

John A. Balboni
NASA Ames Research Center, Moffett Field, CA

National Aeronautics and
Space Administration

Ames Research Center
Moffett Field, California 94035

November 2015

Acknowledgments

The authors are grateful to Dr. Helen Hwang (Science Missions Development Manager, Entry Systems and Technology Division) and Dr. Ethiraj Venkatapathy (Chief Technologist, Entry Systems and Technology Division) for their encouragement and interest in the present work. The authors thank the arc-jet operations crew for their dedicated efforts in assembling, installing, and operating the IHF with the 76 mm nozzle. The present work was supported by NASA Contracts NNA10DE12C to ERC, Inc., NNA15BB15C to AMA, Inc., NNA09DB39C to Jacobs Technology, and by the Outer Planets Program. The critical financial support provided by NASA-SCAP for the arc-jet operational capability at NASA Ames Research Center is gratefully acknowledged.

The present document was typeset using a LaTeX class (`NASA.cls`) developed by Bill Wood and Bil Kleb of NASA Langley Research Center.

Available from:

NASA Center for AeroSpace Information
7115 Standard Drive
Hanover, MD 21076-1320
443-757-5802

Abstract

The design of a new 76 mm (3 inch) nozzle of the Interaction Heating Facility arc jet at NASA Ames Research Center is described. The computational efforts which were an integral part of the preliminary design and characterization of the nozzle are described as well. Details of heat flux measurements made in this new nozzle are provided. Apart from showing the flow characteristics of the nozzle, predictions of stagnation point heat flux are compared against measurements made with a nullpoint calorimeter; the agreement between computation and measurement is found to be good. Unfortunately, pressure measurements could not be made in the first round. Predicted stagnation point pressures and measured heat fluxes are used to establish a provisional operating envelope for the new nozzle. The envelope is shown to enclose relevant heating portions of representative atmospheric trajectories at Venus and Saturn.

1 Introduction

Materials that make up the thermal protection system around an atmospheric entry capsule are tested, qualified, and flight certified in high enthalpy facilities such as arc jets. An arc jet uses a high voltage electric discharge to elevate the temperature (or equivalently, total enthalpy) of the working medium (typically air). This arc-heated gas mixture is then expanded through a converging-diverging nozzle and delivered to an evacuated chamber containing the material coupon to be tested; the coupon is instrumented with thermocouples to gage the thermal response. A comprehensive and lucid description and discussion of US arc jets can be found in the paper of Smith *et al.* [1].

NASA Ames Research Center operates a number of arc-heated facilities in its Arc Jet Complex. The most powerful of these is a 60 MW segmented arc heater called the Interaction Heating Facility (IHF). The IHF heater can be mated to different conical nozzles whose exit diameters are 152 mm (6 inches), 546 mm (21.5 inches) and 762 mm (30 inches), all with a total vertex angle of 20° for the conical diverging section; the choice of nozzle is dictated by the target heat flux and pressures that have to be achieved at the stagnation point of a test coupon. We note here that IHF arc heater can be mated to a semi-elliptic nozzle as well [2].

The main controls in an arc heater are current and flow rate, and these controls are constrained by safe and stable operation of the facility. The limits on the controls are depicted as an operational envelope – a map of heat flux *vs.* pressure at the stagnation point of some reference geometry. Figure 1 shows the operational envelope for the 152 mm nozzle of the IHF and a 25 mm diameter iso-q configuration (a spherical section whose nose radius is the same as the base diameter); the smallest of the nozzles will produce the highest stagnation point environments. Also shown in Fig. 1 are environments along trajectories representative of ballistic entries into Venus and Saturn [3,4]; the peak heating points on these trajectories are shown as closed symbols. Clearly, the operational envelope of the 152 mm nozzle does not encompass these conditions. The lack of a facility to deliver the levels of heat fluxes and pressures representative of Venus and Saturn entries is a concern, and a piecewise testing approach was recommended in the work of Venkatapathy *et al.* [5]. We note here that a special arc heater facility, the Giant Planet Facility [6], was constructed in

support of NASA's Galileo mission to Jupiter. That facility, however, no longer exists.

In view of fact that the existing nozzles – 152 mm (6 inch), 546 mm (21.5 inch), and 762 mm (30 inch) exit diameter – of the IHF do not allow very high levels of pressure (> 1.3 bar) and heat flux (> 2 kW/cm^2), an effort was undertaken to design, construct, and characterize a new nozzle for the IHF. This new nozzle, which has an exit diameter of 76 mm (3 inches), has been installed and tested in the IHF. Owing to its small area ratio (exit area to throat area), the new nozzle will allow testing of thermal protection materials at substantially higher pressures and heat fluxes than the 152 mm nozzle, thus enabling to an extent the replication of pressures and heat fluxes that are representative of entries in Venus, Saturn, and Uranus atmospheres. The present document describes the design of the new nozzle, and the combination of experimental and computational efforts in characterizing its performance.

2 Preliminary Nozzle Design

The preliminary design of a new nozzle for the IHF was predicated on the following ground rules:

1. There would be no change in the arc heater configuration.
2. There would be no change in the throat diameter (60.3 mm or $2\frac{3}{8}$ inches).
3. The length of the new nozzle would be the same as the 152 mm nozzle due to constraints on facility space limitations.

The first ground rule implies that the ranges of arc current, voltage, column pressure, total enthalpy, *etc.* would remain unchanged for the new nozzle. Therefore, the computational methodology (described in a later section) developed by Prabhu *et al.* [7] can be used, without any changes, in the evaluation of various candidate nozzle configurations.

The second ground rule ensures the flow rates through the converging part of the converging-diverging nozzle remain unchanged as well.

The third ground rule provides the only design degree of freedom – the exit diameter of the nozzle. Clearly, the exit diameter has to be greater than the throat diameter of 60.3 mm, but less than 152 mm. Therefore, a number of different exit diameters are possible depending on the choice of total vertex angle of the diverging section, or equivalently a number of different vertex angles are possible depending on the choice of exit diameter. A small vertex angle is preferred because it offers the least amount of gas expansion, which in turn implies less cooling of the arc-heated mixture.

A nozzle exit diameter of 76 mm (3 inches) was chosen as a practical minimum. This choice of exit diameter fixed the total vertex angle at roughly 3.1°. The *geometric* area ratio of this concept nozzle is approximately 1.6, which means that the nozzle exhaust Mach number would be less than approximately 1.8 (based on an isentropic exponent $\gamma = 1.1$).

Flow computations were performed for this 76 mm exit diameter concept nozzle for an arc heater setting of 6000 A and a flow rate of 0.849 kg/s (considered to be close to the highest setting of the IHF). Just as in the case of the 152 mm nozzle, a short (50 mm long) flare of 40° was attached to the end of the nozzle; the flare provides a slightly larger volume

of test gas. The results of these computations are shown in Fig. 2; static temperature contours in the pitch plane of the 76 mm and 152 mm nozzles are shown in Fig. 2a and Mach number contours in Fig. 2b. As can be seen in the figure, the static temperature at the nozzle exit is roughly 7000 K for the 76 mm nozzle and roughly 5500 K for the 152 mm nozzle. Further, the static pressure at the exit of the 76 mm nozzle is roughly 1.7 bar while it is 0.2 bar for the 152 mm nozzle. The increased static temperature and pressure at the nozzle exit suggest that high heat fluxes and pressures are possible at the stagnation point of the material test coupon, which is what is needed for coverage of Venus and Saturn flight trajectories (see Fig. 1). It is interesting to note that the predicted exit Mach numbers for the 76 and 152 mm nozzles are 1.6 and 2.6, respectively. The predicted exit Mach numbers are expected to be lower than simple theory based on equilibrium thermodynamics for two reasons: (1) the "effective" area ratio is smaller than the geometric one due to growth of the boundary layer on the nozzle wall, and (2) the total enthalpy distribution across the radius is *nonuniform*.

The small exit area of the 76 mm nozzle means that test coupon sizes will have to be 25 mm (or smaller) in diameter, implying roughly 10% blockage (by area). Despite the reduction in size of the test coupon, the expected substantial increases in heat flux and pressure at the stagnation point were compelling enough to pursue the design of a new 76 mm nozzle.

3 Final Nozzle Design

The final design of the new nozzle was based on the decision to fix the exit diameter at 76 mm. The 40° flare, as used in the case of the 152 mm nozzle, was not considered for the new nozzle, thus reducing the vertex angle from 3.1° in the concept design to 2.5°. However, two additional requirements were imposed on the final design: (1) the exit end of the nozzle had to be cantilevered, *i.e.*, a small portion of the nozzle would jut out into the test chamber, and (2) provisions would have to be made to have a mirror installed at the exit end of the nozzle so that a fiber pyrometer could be used to monitor the surface temperature of a test coupon.

CAD software from Dassault Systèmes SolidWorks Corp. was used in the detailed design of the nozzle. Figure 3 shows two views – the inlet end (Fig. 3a) and the exit end (Fig. 3b) – of the new 76 mm nozzle. The exit end of the nozzle does project out into the test chamber, and also has provisions for an air-cooled mirror and fiber pyrometer view port, as required. A sectional view of the nozzle is shown in Fig. 4; the arc-heated gas mixture flows from right to left in the figure. The nozzle copper liner is kept cool with high pressure water. The water flows into multiple ports around the center of the outer shell, through water baffles to the copper surface. It then divides and flows along the outside of the liner toward each end, around the baffles and out of the shell through two sets of ports. Figure 5 shows a wireframe outline of the inner contour of the nozzle; the flow direction is from right to left in this figure. In addition, the figure provides a clear view of the arrangement of the fiber pyrometer, the air-cooled mirror, and a test coupon along with the optical paths of how the heated surface of the test coupon is imaged on to the fiber. The wireframe geometry was used to develop grids for flow field simulations.

Since the test coupons to be tested will be small, a specialized sting was also designed.

Figure 6 shows a view of the CAD model of the sting. The sting requires thermal protection, which is provided by wrapping a thin-walled copper tube (6 mm OD) around it. The copper tubing circulates water at high pressure. Further, the sting design is such that the sample end of the sting is protected by an easily replaced sacrificial part.

Although not discussed in the present work, thermal-structural analyses were performed during every stage of the design to determine the water flow rates and stresses within the assemblies; water is necessary to cool the nozzle assembly and stress levels have to be below those levied by facility safety requirements.

Upon completion of the design, the new nozzle was fabricated using a traditional approach, although initially some effort was expended in exploring the possibility of fabricating the nozzle using electroforming.

4 Test Conditions and Measurements

After the initial integration and system tests, a dedicated test entry (IHF333) in August/September of 2013 was focused on the first round of characterization of the new 76 mm nozzle. The run matrix for this test entry is shown in Table 1. The table entries are not chronologically arranged. Rather, they are ordered in increasing arc current, and then by increasing arc column pressure. Repeat runs are grouped together, and these groups are separated by dashed lines in the table. In all there are 21 distinct heater conditions in the first round of characterization of the new nozzle, and an attempt was made to systematically step through a range of flow rates for arc current ranging from 2000 A to 6000 A.

4.1 Arc heater

A key measurement of performance of the arc heater is bulk enthalpy, which is also a critical parameter in flow simulations. The bulk enthalpy, measured by energy balance [8], for each of the cases in the test matrix is shown in Table 1; this measured bulk enthalpy is abbreviated as EB2, which is short for Enthalpy By Energy Balance. We note here that the energy balance method measures heat loss through the entire system – arc heater and nozzle – by change in temperature of water used to cool the system. For reasonably high enthalpies, the reported uncertainties are roughly ±6-7%. Note: measurements of bulk enthalpy can have non-negligible variability and scatter, and this scatter/variability should perhaps be factored in when more precise results are desired or for arc-heater forensics.

In a predictive framework built around flow simulation tools, the bulk enthalpy is correlated against a sonic flow parameter, σ, which is defined as:

$$\sigma = \frac{\dot{m}_{\text{total}}}{A_{\text{throat}} P_{\text{arc}}} \tag{1}$$

where $\dot{m}_{\text{total}}$ is the total mass flow rate, A_{throat} is the throat area, and P_{arc} is the arc column pressure. The sonic flow parameter has units of $\frac{\text{s}}{\text{m}}$. The correlation is a power law:

$$H_{\text{bulk}} = \left(\frac{C}{\sigma}\right)^{\beta} \tag{2}$$

where the constants β and C are determined using measured values of H_{bulk} and σ. The correlation (Eq. 2), in the absence of EB2 measurements or presence of faulty EB2 measurements, provides a convenient way to estimate bulk enthalpy from measurements of flow

rate and arc column pressure alone. For the current predictive purposes, it is better to rely on the simple correlation offered by Eq. 2 above.

There are at least three different sources for the parameters β and C: (1) the work of Winovich [9], which has values of 2.519 and 123, (2) the work of Shepard *et al.* [10], which has values of 1.971 and 158.7, and (3) a more recent effort of Thompson *et al.* [11], using a much larger data set of bulk enthalpy measurements, which has values of 2 and 155.8. The value of 2 for the parameter β makes dimensionally correct the correlation in Eq. 2. Note: the bulk enthalpy based on the Winovich correlation is usually what is reported in run summaries.

The measured bulk enthalpies (EB2) shown in Table 1 are plotted against the sonic flow parameter, σ (Eq. 1) in Fig. 7. In Fig. 7a, the data are fit using the Winovich value for β in Eq. 2, while in Fig. 7b, the same data are fit using a value of 2 for β. In both cases, the constant C is determined from the curve fitting procedure. In the former case, C has a value of 123.7, and in the latter case, C has a value of 169.5. In either case, the residuals from the curve fitting procedure lie within a ± 5 MJ/kg band (the 95% prediction interval). In Figs. 7a and 7b, the power law fit is shown as a solid line, measurements as open red symbols, the 95% confidence intervals as dashed lines, the prediction intervals as dotted lines, and the residuals as open green symbols. For the 76 mm nozzle tests, neither curve fit is superior to the other.

The curve fitting procedure is repeated using a large dataset of EB2 measurements. The results are shown in Fig 8; the closed symbols are historical measurements for the arc heater of the IHF with all nozzles, 76-, 152-, 330-, and 546-mm exit diameters, and the open symbols are from the 76 mm nozzle tests. The values of C are now 118.6 and 159.6 for the Winovich and Thompson *et al.* fits, respectively. With the increased number of data points, the curve fit form of Thompson *et al.* is marginally superior to that of Winovich.

The EB2 measurements from the first round of characterization of the 76 mm nozzle are biased high compared to the historical mean, but the scatter of ± 5 MJ/kg is consistent with previous measurements. This level of scatter in bulk enthalpy translates to a 20% uncertainty in heat flux measurements since heat flux is directly proportional to stagnation enthalpy.

A plausible reason for large scatter in EB2 measurements is the run-to-run variation in arc column pressure (measured at the middle of the column). Using Eqs. 1 and 2, the linear sensitivity of bulk enthalpy is related to the measurement uncertainties in arc column pressure and flow rates as:

$$\frac{\Delta H_{\text{bulk}}}{H_{\text{bulk}}} = \beta \frac{\Delta P_{\text{arc}}}{P_{\text{arc}}} - \beta \frac{\Delta \dot{m}_{\text{total}}}{\dot{m}_{\text{total}}} \tag{3}$$

If the flow rates are measured precisely, then the uncertainty in bulk enthalpy goes directly as the uncertainty in column pressure with exponent of the power law of Eq. 2 as the constant of proportionality. Furthermore, the choice of fit – Winovich, or Thompson *et al.* – amplifies the column pressure uncertainties differently.

4.2 Instrumentation

A nullpoint calorimeter (Fig. 9) was swept (in both the forward and backward directions) through the free jet. However, measurements of stagnation pressure using a pitot probe

were confined to just the centerline of the free jet. These measurements along with an "effective radius" for the nullpoint calorimeter can be used to determine the enthalpy at the centerline of the free jet. Both probes are 15° sphere-cone geometries, each with a nose radius of 4.6 mm. The nullpoint probe has a 1.5 mm (radius) sensor at the tip, and the pitot probe has a 0.8 mm (radius) orifice at the tip.

The measured values of heat flux and pitot pressure at the nozzle centerline from the first round of characterization of the nozzle flow are given in Table 2. All measurements were made at a distance of 13 mm (0.5 inch) from the exit plane of the nozzle. The jet centerline values obtained from both forward and backward sweeps of the nullpoint probe are listed along with their simple arithmetic average. For two runs (#15 and #16) there were at least two sweeps of the nullpoint through the jet.

For the 2000 A heater setting, despite the larger arc column pressure in Run #11, the measured heat fluxes are *lower* than those in Run #1. The behavior is similar in Run #7 for a 4000 A heater setting. For the 3500 A heater setting, there is as much as 50% difference between the low and high values of measured heat flux. For the 6000 A heater setting, this difference is 25%.

In the first round of characterization of the new nozzle, pressure measurements could not be made at almost all conditions because the tips of the 9 mm (diameter) 15° sphere-cone probes melted at high heat fluxes. The pressure transducer of the water-cooled pressure probe was located far back from the orifice, and thus probably had too little dwell time for equilibration. In the next round of characterization (planned for Fall 2015), the transducer will be moved closer to the orifice to reduce the equilbration time.

The first round of characterization was focused on learning how to make measurements in thermal environments that are significantly higher than those of the larger nozzles of the IHF, and also to develop a provisional test envelope for the new nozzle. Therefore, the present work makes no attempt to quantify uncertainties in measurements, saving this analysis until after completion of the second round of characterization.

5 Simulation Methodology

Having discussed the design of the nozzle, the test conditions and instrumentation, we turn next to the simulation methodology employed in tandem with measurements during the characterization of the new nozzle. Numerical simulations of arc-heated flows are now an integral part of testing, with computation methods being utilized in the design of the test and/or test articles, in pre-test predictions of flow environments (primarily to estimate exposure time for test articles), and post-test analysis (including shape change, if any, of test articles). Since the new 76 mm nozzle uses the same 60 MW constricted arc heater as before, the computational methodology/process developed previously for the other larger nozzles will be applicable to the new nozzle as well.

The computational analysis framework developed by Prabhu *et al.* [7] uses a simplified approach to the simulation of the expansion of arc-heated flow by eliminating the arc heater in the modeling, *i.e.*, the computational domain, which starts at the plenum (assuming that one is established), includes just the nozzle and the free jet. It is then sufficient to know the thermochemical state of the arc-heated gas in the plenum; at high operating arc column pressures (1 bar or greater), the likelihood is high that the arc-heated mixture in the plenum

is in a state of local thermodynamic equilibrium.

A feature of the arc heater of the IHF is that the stagnation enthalpy is not uniform across the face of the plenum. The distribution of stagnation enthalpy across the inflow face is determined by sweeping the free jet with nullpoint and pitot probes, computing the total enthalpy from the combination of stagnation point heat flux and pressure (Eq. 4), and then tracing the streamlines back from the jet to the plenum.

$$\dot{q}_{\text{stag}}(r) = K \frac{\sqrt{p_{\text{stag}}}}{\sqrt{R_{\text{eff}}}} H(r) \tag{4}$$

where r is the radial coordinate measured from the nozzle centerline, and K is a constant for the gas mixture (air and argon typically in the IHF).

$$\frac{1}{K} = \frac{c_{\text{air}}}{K_{\text{air}}} + \frac{c_{\text{Ar}}}{K_{\text{Ar}}} \tag{5}$$

The values for K_{air} ($= 3.904 \times 10^{-4}$ kg/m$^{\frac{3}{2}}$·s·Pa$^{\frac{1}{2}}$) and K_{Ar} ($= 5.513 \times 10^{-4}$ kg/m$^{\frac{3}{2}}$·s·Pa$^{\frac{1}{2}}$) are taken from the work of Zoby [12]. The mass fractions of air and argon are, respectively, c_{air} and c_{Ar}:

$$c_{\text{air}} = \frac{\dot{m}_{\text{air}}}{\dot{m}_{\text{total}}}, \; c_{\text{Ar}} = \frac{\dot{m}_{\text{Ar}}}{\dot{m}_{\text{total}}} \tag{6}$$

and $\dot{m}_{\text{total}}$ is the total mass flow rate:

$$\dot{m}_{\text{total}} = \dot{m}_{\text{air}} + \dot{m}_{\text{Ar}} \tag{7}$$

5.1 Modeling details

The axisymmetric version of an in-house flow solver, DPLR [13], has been used in all the computations for which results are reported in the present work. A 6-species gas mixture (N_2, O_2, NO, N, O, Ar) is representative of the flow and ionization is neglected. The gas mixture is assumed to be in thermal and chemical nonequilibrium, *i.e.*, the translational and vibrational temperatures are distinct, and there is finite-rate chemistry in the nozzle expansion. In view of the high operating pressures and small area ratio of the new nozzle, the consideration of nonequilibrium is probably unnecessary. Although thermal equilibrium can easily be imposed on the problem via the options available in DPLR, chemical equilibrium cannot. The workaround for chemical equilibrium is to simply scale up the forward reaction rates by 6 orders of magnitude. Finally, since the arc heater and nozzle are water cooled, the nozzle wall is assumed isothermal and fully catalytic to recombination of gas-phase atoms.

Using the bulk enthalpy from Eq. 2, the first step is to construct a profile of stagnation enthalpy across the face of the plenum. Based on previous sweeps (with a nullpoint calorimeter and a pitot probe) of the free jets of various nozzles, a simple Gaussian distribution is assumed (see Ref. 7 for details).

The final step is to use the measured flow rates, the bulk enthalpy estimate, and profile of stagnation enthalpy (and mass flux, if necessary) in a software utility program, NOZZLE_THROAT_CONDITIONS [14], to generate the profiles of species mass densities, temperature, and velocity in the form required by DPLR. Flow computations are then performed for a given nozzle geometry.

5.2 Computational domain

The pitch plane profile of the new 76 mm (exit diameter) nozzle is shown in Fig. 10. The nozzle has a convergent section that is almost identical to the other nozzles used in the IHF. However, the divergent section has a cone semi-vertex angle of 1.26°, which is much smaller than the 10° angle of all the other nozzles used in the IHF. The computational domain includes the plenum, the nozzle (blue lines), and the free jet (red lines). Supersonic outflow boundary conditions (zeroth-order extrapolation) are employed on the free jet domain.

A single mesh was generated using a commercial tool, GridPro [15], for the two-zone computational domain shown in Fig. 10.

Once the flow field has been computed, the solution is queried at points along the nozzle centerline, and the values of density, axial velocity, kinetic and vibrational temperatures, and mass fractions are extracted; in the present work, only one axial location — 13 mm (0.5 inch) from the nozzle exit plane — was considered. These extracted values are used as *uniform* freestream conditions for the probes (any geometry). Strictly speaking, the probe geometry and test box should be included in the simulation, but for the first round of characterization of this new nozzle, the simpler approach of a standalone probe was preferred.

6 Computational Results

Flow computations were performed using v4.03.1 of Dplr for all cases in the test matrix (Table 1), excluding the repeat runs, disregarding the fact that pressure measurements were not successful in the first round of characterization of the nozzle. This is partly based on the confidence in predicting stagnation point pressure to within ±5% of measurements in test campaigns in the other nozzles of the IHF. The process described in the work of Prabhu *et al.* [7] is used unchanged in the simulations.

Results are presented in three parts. In the first part, the computed characteristics of the nozzle are presented for each current setting of the arc heater. In the second part, comparisons are made between predicted stagnation point heat fluxes and measurements using a nullpoint calorimeter. An attempt has also been made to compute the flow on a hemisphere whose radius is equivalent to that of the nullpoint calorimeter. This hemispherical radius is the "effective radius" shown in Eq. 4. In the third part, an operational envelope of the new nozzle is estimated.

6.1 Nozzle flow characteristics

The flow characteristics chosen for display in the present work are the centerline distributions of static pressure, frozen Mach number, temperature, and mass fraction of atomic nitrogen. In Figs. 11 through 16, distributions are shown for arc currents of 2000, 3000, 3500, 4000, 5000, and 6000 A, with variations in arc column pressure (and flow rates). For all cases, the nozzle exit Mach number is roughly 1.6, which is smaller than the expected value of 1.8 based on an isentropic exponent between 1.1 and 1.2 for an area ratio of 1.6. This difference is most likely due to boundary-layer growth and nonuniformity in total enthalpy of the stream. Furthermore, the sharp inflections in the curves (in the neighborhood of 40-45 mm from the nozzle exit plane) suggest where the test rhombus closes.

In Fig. 17, the pitch plane contours of frozen Mach number are shown for a case that is not in the test matrix (Table 1). This result was readily available for inclusion here, and the point of the contour plot is to provide an idea of the size of the first test rhombus where one typically tests materials. The size of the rhombus gives an idea of the largest diameter of the test coupon, and also gives an idea of where the test article should be placed from the nozzle exit plane. From the results, one can infer that the test coupon size should be under 25 mm (1 inch) in diameter, and should be tested as close as possible to the nozzle exit plane.

6.2 Calorimetry

Surface distributions of pressure and heat flux for several conditions in the test matrix (Table 1) are shown in Figs. 18 through 24 for the nullpoint geometry (Fig. 9), which is a 4.6 mm nose radius (without the flat sensor) sphere-cone (15 cone angle).

Consider the results shown in Fig. 18 for the 2000 A heater setting. The computed pressures and heat fluxes vary in proportion (more or less) to the arc column pressure. However, the measured heat fluxes at higher flow rates (equivalently higher column pressures) show a *decrease*, suggesting that the measurements at both conditions of Run #11 are significantly lower by as much as 30%. However, there is good agreement between measurement and computation for all conditions of Run #1. For these cases of Run#1 the predicted stagnation point heat fluxes lie well within an assumed $\pm 15\%$ uncertainty in measurements. In contrast, *all* three conditions of Run #14 have measurements that are substantially lower than predictions. For arc currents greater than 3000 A, there is great improvement in the agreement between computations and measurements. Figure 24 makes clear the amount of scatter (roughly 25% between average high and low values) at the highest heater setting of 6000 A. Given that measurements at 3000 and 3500 A were made *after* the nullpoint calorimeter was exposed to high heat fluxes at 6000 A, we speculate that the lower than expected heat fluxes at lower arc currents is due to some sort of "hysteresis" effect. We note that computations for *all* heater settings were performed without any change to the simulation process, *i.e.*, the simulation process was not altered to match the measured heat fluxes. Furthermore, computations showed only a small sensitivity to arc column pressure – the basis for the sonic flow correlation of bulk enthalpy.

As mentioned earlier, there are no pressure measurements to compare against and gain absolute confidence in the simulation methodology. The various issues with measurements will have to explored at the same heater settings in the second round of characterization.

6.3 Operational envelope

There are lower and upper limits to both the arc current and flow rates for a given arc-jet facility; the limits are driven by arc stability and facility operational safety. These limits are traditionally depicted on a heat flux *vs.* pressure map for a combination of current and mass flow settings of the arc heater; the heat flux and pressure are at the stagnation point of a *reference* geometry. Using simple nozzle area ratio models with equilibrium thermodynamic properties, the thermodynamic state of the expanded arc-heated mixture can be predicted at the exit of the nozzle. Using this thermodynamic state as "freestream conditions," the pressure and cold-wall heat flux at the stagnation point of the reference

geometry are computed using a simplified version (*e.g.*, Eq. 4) of the Fay-Riddell correlation [16].

A 25 mm (1 inch) diameter iso-q geometry is chosen as the reference geometry for defining the operational envelope of the new 76 mm (3 inch) diameter nozzle; an iso-q geometry is a spherical section whose geometric radius is the same as the base diameter. The reference geometry diameter of 25 mm is appropriate for the size of the exit of the nozzle, and the "blockage" (defined as the ratio of the nozzle exit area to the cross sectional area of the test geometry) is 11%, which is less than the suggested upper limit of 25%.

First, Eq. 4 can be restated as:

$$\dot{q}_{\text{stag}} \propto \frac{1}{\sqrt{R_{\text{eff}}}} \tag{8}$$

Next, since the "freestream conditions" are the same for the nullpoint calorimeter and the reference geometry, it follows from Eq. 4 that heat flux at the stagnation point of the reference geometry (25 mm iso-q) is related to that of the nullpoint by

$$\dot{q}_{\text{stag,isoq}} = \left(\frac{\sqrt{R_{\text{hemi}}}}{\sqrt{R_{\text{eff,isoq}}}} \right) \left(\frac{\sqrt{R_{\text{eff,nullpt}}}}{\sqrt{R_{\text{hemi}}}} \right) \dot{q}_{\text{stag,nullpt}} \tag{9}$$

The "effective radius" of the nullpoint geometry is ≈18 mm. The two geometries are compared in Fig. 25, and the distributions of surface pressure and cold-wall heat flux at free stream conditions corresponding to Run #3/Condition #2 of the test matrix (Table 1) are shown in Fig. 26. The stagnation point pressures are in excellent agreement, while the stagnation point heat fluxes are within 5% of each other. More precise agreement can be achieved with more precision in the value of the radius of the hemispherical part of the hemisphere-cylinder geometry. However, no attempt is made in the present work to achieve perfect agreement.

The "effective radius" of the iso-q geometry is ≈23 mm. This value is read off a graph provided in the report of Zoby and Sullivan [17]. The two geometries are compared in Fig. 27, and the distributions of surface pressure and cold-wall heat flux at free stream conditions corresponding to Run #3/Condition #2 of the test matrix (Table 1) are shown in Fig. 28. The stagnation point pressures are in excellent agreement, while the stagnation point heat fluxes are within 3% of each other. As with the nullpoint calorimeter comparison, more precise agreement can be achieved with more precision in the value of the radius of the hemispherical part of the hemisphere-cylinder geometry. However, no attempt is made in the present work to achieve perfect agreement.

The stagnation point heat flux and pressure envelopes are plotted in Fig. 29 for the 152 mm (6 inch) and 76 mm (3 inch) nozzles. The envelope for the 76 mm nozzle is notional and is based on scaling from the 152 mm nozzle. It is important to note here that the open symbols shown are a combination of *measured* heat fluxes and *predicted* pressures. This inconsistency is due to lack of pressure measurements in the first round of characterization, and will be fixed after the second round of characterization scheduled for Fall 2015. Also shown in the figure are environments along representative trajectories of atmospheric flight at Venus and Saturn. The new nozzle provides good coverage of the region around the peak heating points of these trajectories. However, meeting the peak dynamic pressure target (much reduced heat flux) will require the use of other arc-jet facilities [4].

7 Concluding Remarks

The present work documents some of the work done in the design, development, installation, and characterization of a new 76 mm (exit diameter) nozzle of the IHF at NASA Ames Research Center. From the first round of characterization, which was supported by a computational process developed for arc-heated flow fields, a provisional operating envelope has been constructed for this nozzle. This provisional envelope is shown to encompass representative trajectories of atmospheric entries into Venus and Saturn.

Despite the lack of pressure measurements, there is good agreement between predictions and measurements at arc currents beyond 3500 A. It is anticipated that improvements to both operations and instrumentation in the second round of characterization will help sharpen the operating envelope of the new nozzle.

Although not shown in the present document, examination of the kinetic and vibrational temperature fields showed that the two temperatures were virtually identical. Essentially this means that for the operating pressure of the arc heater, a single temperature model is sufficient for the purposes of analysis.

The few remaining studies that have been deferred to the next round of characterization are:

1. Inclusion of add air: The method for lowering the bulk enthalpy of the arc-heated mixture is to add room temperature air (also called "add air") *after* the arc column. Adding room temperature air not only reduces the bulk enthalpy, it also raises the stagnation point pressure. Adding air is accomplished by attaching an additional special segment after the electrode package. In the first round of characterization, this special segment was not used, and "low" enthalpy operation was not explored."Low" enthalpy exploration is perhaps not entirely necessary to establish high-temperature performance of thermal protection materials. However, high pressure tests (achieved using the "add air" package) at slightly reduced heat fluxes might be useful in exploring performance boundaries of the materials. The analysis process then requires small changes for these cases. Although not explored in the present work, the necessary steps are documented in the work of Prabhu *et al.* [7].

2. Inclusion of the test box and diffuser inlet: This expansion of the computational domain will give a better idea of the size of the first test rhombus, which drives the size and shape of the test coupon. Furthermore, if indeed there is a second test rhombus in the underexpanded nozzle, the possibility of testing in the second rhombus could be explored. The assumption is that pressure and heat flux measurements made at several points along the nozzle axis and away from the nozzle exit plane will help define the closure of the first test rhombus.

3. Exploration of ionization: Usually ionization is neglected, especially since simulations for the larger nozzles of the IHF show that free electron mole fractions are quite low in the free jet. At high arc column pressures, which is the typical mode of operation of the IHF, ionization probably does not matter. Nevertheless, it would be worthwhile determining the ionization level of the free jet.

References

1. Smith, D. M., Felderman, E. J., Shope, F. L., and Balboni, J. A., Arc-Heated Facilities, in *Advanced Hypersonic Test Facilities* (eds. F. K. Lu and D. E. Marren), *Progress in Astronautics and Aeronautics, Vol. 198*, pp. 279-314, AIAA, 2002.

2. Loomis, M. P., Polsky, S., Venkatapathy, E., Prabhu, D., and Hui, F. C. L., "Arc-jet Semi-Elliptic Nozzle Simulations and Validation in Support of X-33 TPS Testing," AIAA Paper 98-0864, 36th AIAA Aerospace Sciences Meeting, Reno, NV, January, 1998.

3. Prabhu, D., Allen, G., Hwang, H., Cappuccio, G., Spilker, T., and Moses, R., "Ballistic Entries at Venus," NASA/TM-2014-218310, April 2014.

4. Prabhu, D., Allen, G., Hwang, H., Cappuccio, G., Spilker, T., and Moses, R., "Atmospheric Entry Studies for Saturn Missions: 45° Sphere-Cone Rigid Aeroshells and Ballistic Entries," 10th International Planetary Probe Workshop, San Jose State University, San Jose, CA, June 1721, 2013.

5. Venkatapathy, E., Laub, B., Hartmann, G. J., Arnold, J. O., Wright, M. W., and Allen, G. A., "Selection and Certification of TPS: Constraints and Considerations for Venus Missions," 6th International Planetary Probe Workshop, Atlanta, GA, June 2008.

6. Winovich, W. and Carlson, W., "The Giant Planet Facility," 25th ISA Symposium, Anaheim, CA, May 1979.

7. Prabhu, D., Saunders, D., Oishi, T., Skokova, K., Santos, J., Fu, J., Terrazas-Salinas, I., Carballo, E., and Driver, D., "CFD Analysis Framework for Arc-Heated Flowfields, I: Stagnation Testing in Arc-jets at NASA ARC," AIAA Paper 2009-4080, 41st AIAA Thermophysics Conference, San Antonio, TX, June 2225, 2009.

8. Hightower, T. M., Balboni, J. A., MacDonald, C. L., Anderson, K. F., and Martinez, E. R., "Enthalpy by Energy Balance for Aerodynamic Heating Facility at NASA Ames Research Center Arc Jet Complex," 48th International Instrumentation Symposium, The Instrumentation Systems, and Automation Society, Research Triangle Park, NC, May 2002.

9. Winovich, W., "On the equilibrium sonic flow method for evaluating electric-arc air-heater performance," NASA TN D-2132, March 1964.

10. Shepard, C. E., Milos, F. S., and Taunk, J. S., "A sonic flow equation for electric arc jets," AIAA Paper 1993-3183, July 1993.

11. Thompson, C. S., Prabhu, D., Terrazas-Salinas, I., and Mach., J. J., "Bulk Enthalpy Calculations in the Arc Jet Facility at NASA ARC," AIAA Paper 2011-3475, 42nd AIAA Thermophysics Conference, Honolulu, HI, June 2730, 2011.

12. Zoby, E. V., "Empirical Stagnation-Point Heat-Transfer Relation in Several Gas Mixtures," NASA TN D-4799, Oct. 1968.

13. Wright, M. W., White, T., and Mangini, N., "Data Parallel Line Relaxation (DPLR) Code User Manual Version 4.01.1," NASA/TM-2009-215388, 2009.

14. Saunders, D. A., and Gökçen, T., "Nozzle Throat Conditions for Arc-jet Computations (1) Axisymmetric," ELORET Report TSA-01-DB2-1-2008, October 2008.

15. Program Development Company, 300 Hamilton Avenue, Suite 409, White Plains, NY 10601, USA.

16. Fay, J. A., and Riddell, F. R., "Theory of Stagnation Point Heat Transfer in Dissociated Air," *Journal of Aeronautical Sciences*, Vol. 25, No. 2, 1958, pp. 73–85.

17. Zoby, E. V., and Sullivan, E. M., "Effects of Corner Radius on Stagnation-Point Velocity Gradients on Blunt Axisymmetric Bodies," *Journal of Spacecraft and Rockets*, Vol. 3, No. 10, pp. 1567–1567, 1966.

Table 1: Run conditions from the first round of characterization of the 76 mm nozzle.

Target	**Run**	**Cond.**	$\mathbf{I_{arc}}$	$\mathbf{V_{arc}}$	$\mathbf{P_{arc}}$	$\mathbf{\dot{m}_{air}}$	$\mathbf{\dot{m}_{Ar}}$	**EB2**[a]
	#	#	A	V	kPa	g/s	g/s	MJ/kg
	1	1	2010	2348	97	100	12	22.0
	1	2	2010	3018	146	150	15	20.1
2000 A	1	3	2008	3602	193	200	18	18.7
	11	1	1998	4125	238	250	21	17.2
	11	2	2027	5057	329	350	27	15.7
	14	1	2986	3798	251	250	21	20.4
3000 A	14	2	2995	4628	346	350	27	18.5
	14	3	2998	5378	439	450	33	17.1
3500 A	2	1	3498	3722	260	250	21	22.7
	10	2	3485	5230	452	450	33	18.5
3500 A	15	1	3487	5284	456	450	33	18.8
	16	1	3494	5233	451	450	33	18.6
	10	5	3592	6445	640	650	45	17.1
3500 A	14	4	3498	6502	635	650	45	16.6
	2	2	3704	6457	651	651	45	17.5
4000 A	7	1	3982	3654	263	250	21	24.2
	10	1	3991	3647	264	250	21	23.8
4000 A	7	2	3993	5126	461	450	33	20.2
	7	4	3994	6342	650	650	45	18.0
	6	2	4990	3572	270	250	21	24.7
5000 A	7	3	4980	4974	475	450	33	22.0
	8	1	4990	6142	673	650	45	20.1
6000 A	6	1	5991	3546	277	250	21	26.3
	10	3	5987	4884	489	450	33	23.7
	4	1	5979	6023	692	650	45	22.5
	10	4	5983	6020	693	650	45	22.3
	7	5	5985	6000	688	650	45	22.4
	3	1	5987	6006	690	650	45	22.4
6000 A	2	3	5988	6042	696	650	45	23.1
	6	3	5988	6005	689	650	45	22.5
	8	2	5992	6009	690	650	45	22.8
	5	1	5998	6027	693	650	45	22.9
	12	1	5998	6032	693	650	45	22.7
	13	1	5979	6054	697	650	45	22.5
	16	1	5991	6026	692	650	45	22.3
6000 A	3	2	5990	6743	835	790	53	23.4

[a]Enthalpy By Energy Balance

Table 2: Centerline measurements of heat flux and pitot pressure for the 76 mm nozzle from the first round of characterization.

Target	**Run** #	**Cond.** #	$\dot{q}_{CL}$ W/cm2			p_{CL} kPa		
			Fwd.	Bwd.	Ave.	Fwd.	Bwd.	Ave.
	1	1	2774	2839	2806			
	1	2	3396	3506	3451			
2000 A	1	3	3396	4048	3722			
	11	1	3241	3261	3251			
	11	2	3456	3463	3460			
	14	1	3676	3669	3673			
3000 A	14	2	3732	4013	3873			
	14	3	3795	4353	4074			
3500 A	2	1	5250	5282	5266			
	10	2	5362	5362	5362			
	15	1	4675	5225	4950			
			5243	6946	6095			
3500 A	16	1	5383	5386	5385			
			7555	7693	7624			
	10	5	6224	6224	6224	475	448	462
3500 A	14	4	5174	5621	5398			
	2	2	7777	7628	7703			
4000 A	7	1	4940	4940	4940			
	10	1	5235	5245	5240			
4000 A	7	2	8292	8292	8292			
	7	4	7714	5690	6702			
	6	2	6278	5552	5915			
5000 A	7	3	7803	6152	6978			
	8	1	8697	8810	8754			
6000 A	6	1	6880	5526	6203	208		
	10	3	8025	8434	8230			
	4	1	10367	10570	10468			
	10	4	9463	9313	9388			
	7	5	10765	10765	10765			
	3	1	10735	9696	10215			
6000 A	2	3	10811	9711	10261			
	6	3	11460	11802	11631			
	8	2	10191	10324	10258			
	5	1	10976	12032	11504			
	12	1	8728	8805	8767			
	13	1	8522	8505	8514			
	16	1	9111	10435	9773			
			11092	11384	11238			
6000 A	3	2	11821	10973	11397			

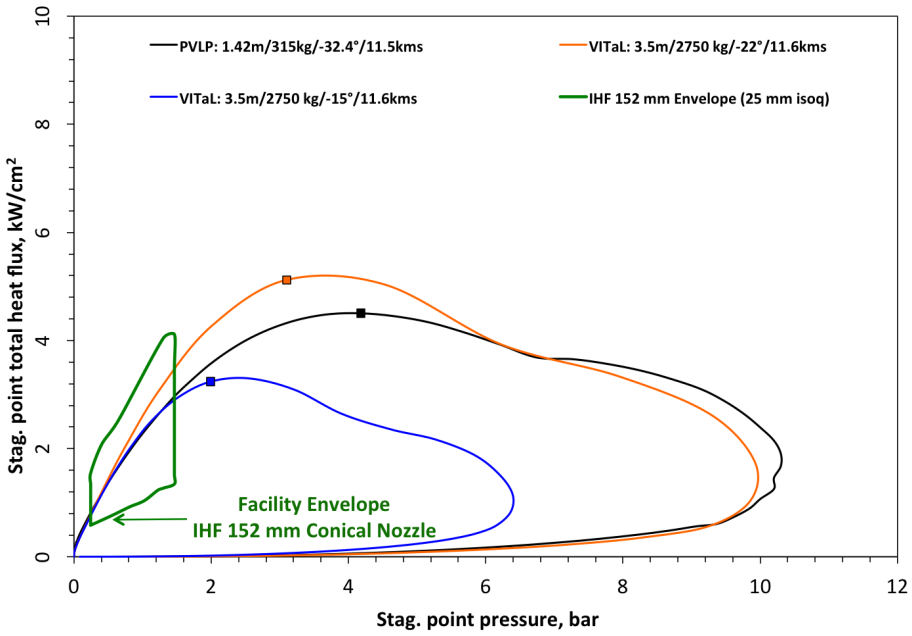

(a) Venus trajectories

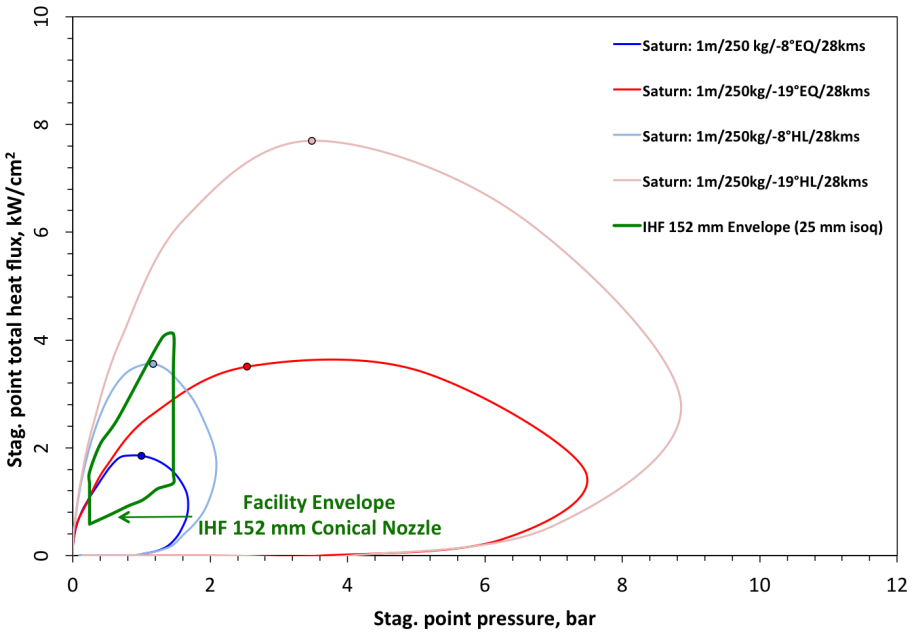

(b) Saturn trajectories

Figure 1: Operating envelope (stag. point heat flux *vs.* pressure) of the 152 mm nozzle of the IHF is shown along with representative trajectory environments for Venus and Saturn atmospheric entries. The closed symbols shown indicate the points of peak heating along the trajectories. PVLP: *P*ioneer-*V*enus *L*arge *P*robe, and VITaL: *V*enus *I*ntrepid *T*essera *L*ander.

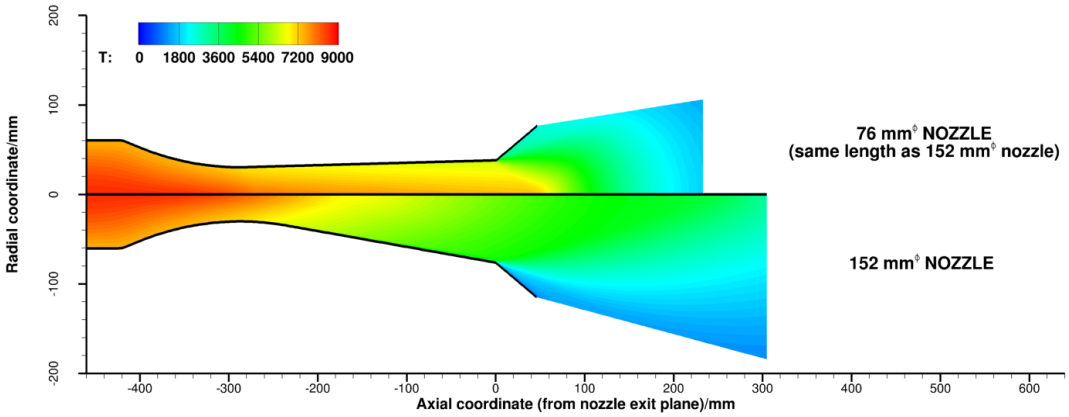

(a) Static temperature

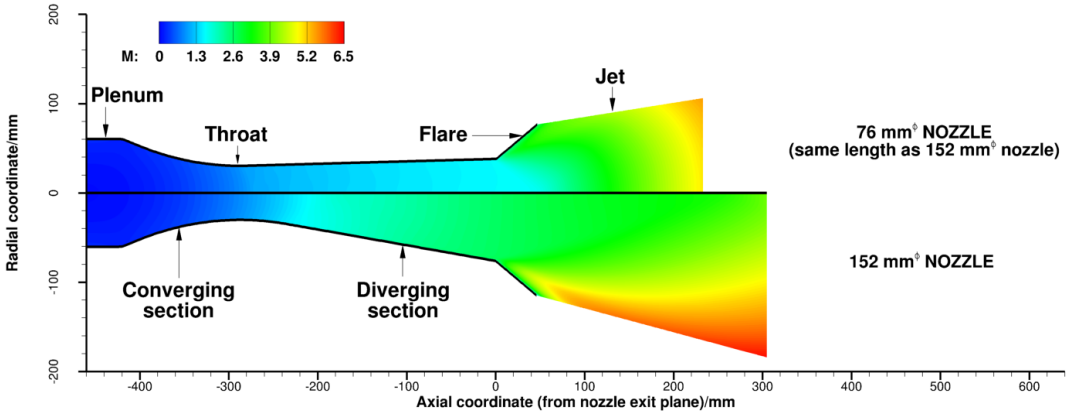

(b) Mach number

Figure 2: Static temperature and Mach number contours for the concept 76 mm nozzle (top half of each figure) and 152 mm nozzle (bottom half of each figure) at the same heater conditions - $I_{\text{arc}} = 6000$ A, $\dot{m}_{\text{total}} = 849$ g/s, and $P_{\text{arc}} = 886$ kPa. Both nozzles have the same length, and both are equipped with a 40° flare.

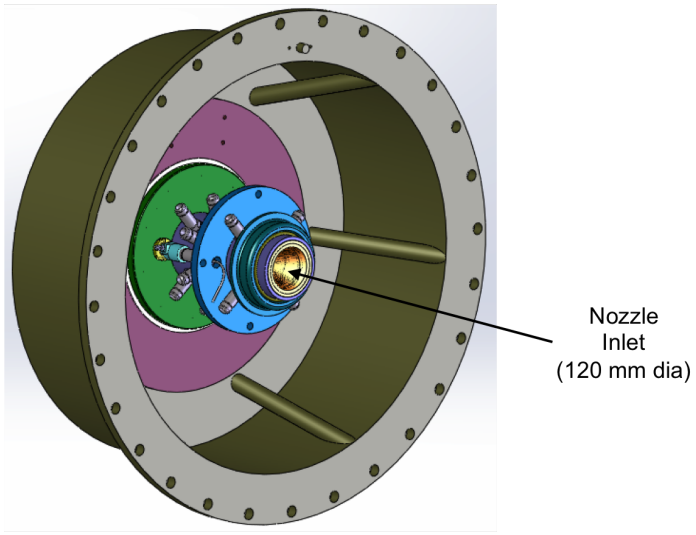

(a) Inlet end

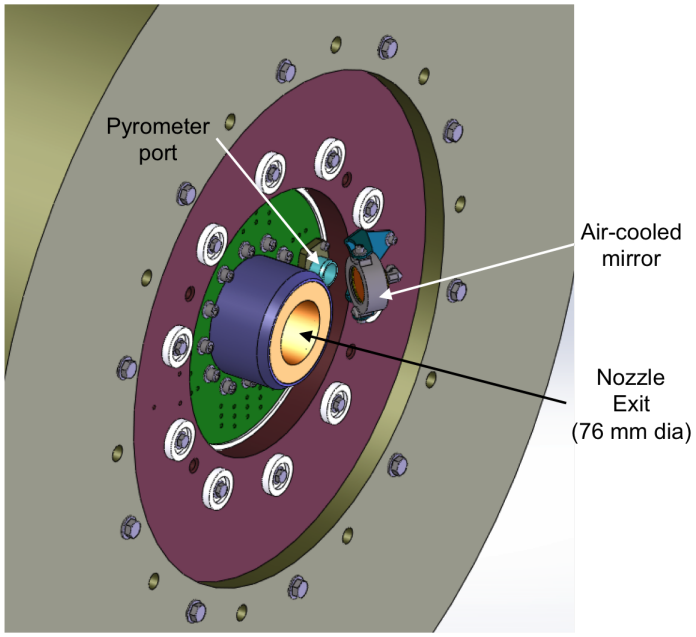

(b) Exit end

Figure 3: CAD model views of: (a) the inlet end of the 76 mm nozzle in its test chamber mounting tub, with arc jet column removed, and (b) the exit end of the nozzle projecting into the test chamber. An air-cooled mirror and pyrometer view port are also visible at the upper right.

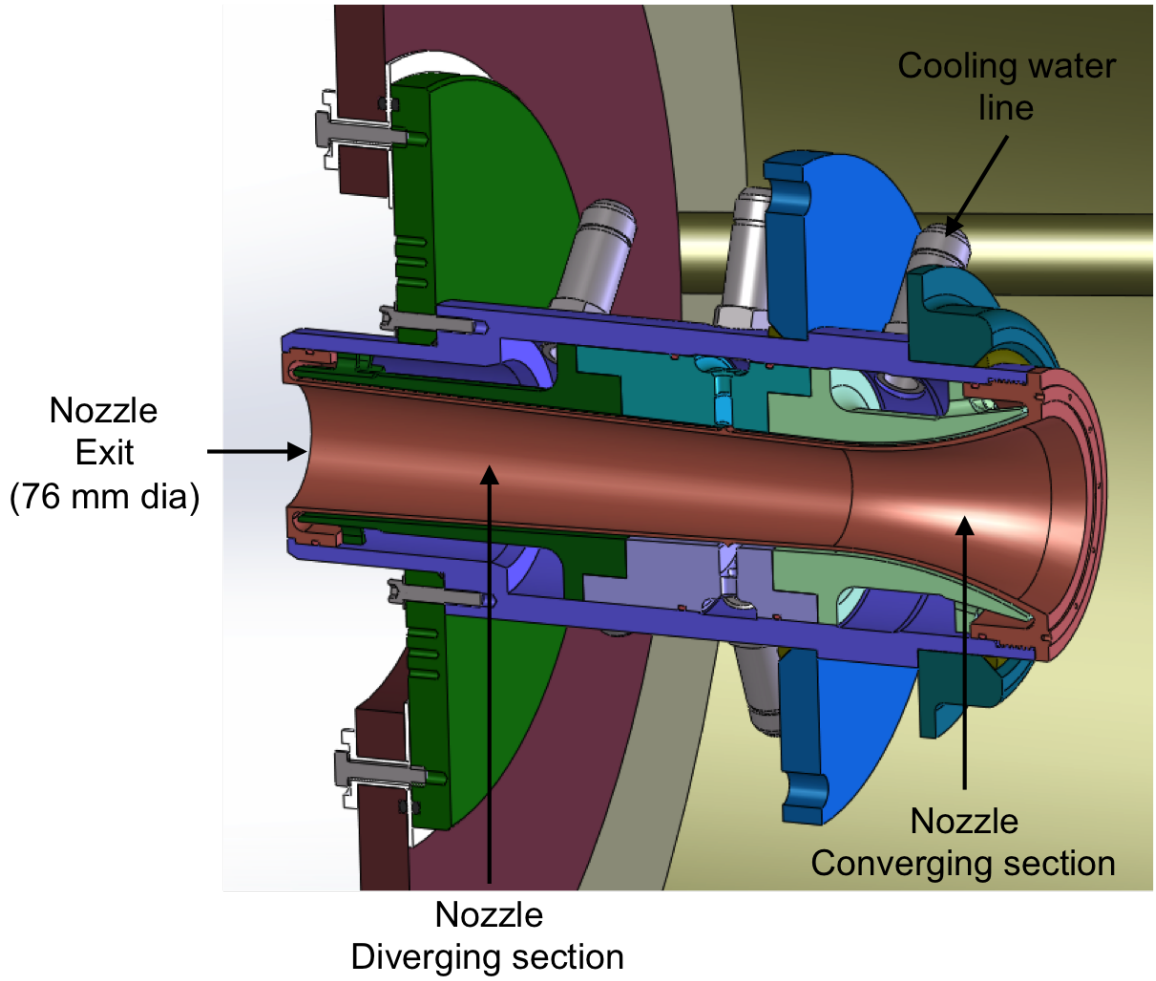

Figure 4: CAD model sectional view of the 76 mm nozzle. The flow is from right to left, *i.e.*, the exit of the nozzle is at the left end of the sectional view. The nozzle copper liner is kept cool with high pressure water. The water flows into multiple ports around the center of the outer shell, through water baffles to the copper surface, it then divides and flows along the outside of the liner toward each end, around the baffles and out of the shell through two sets of ports.

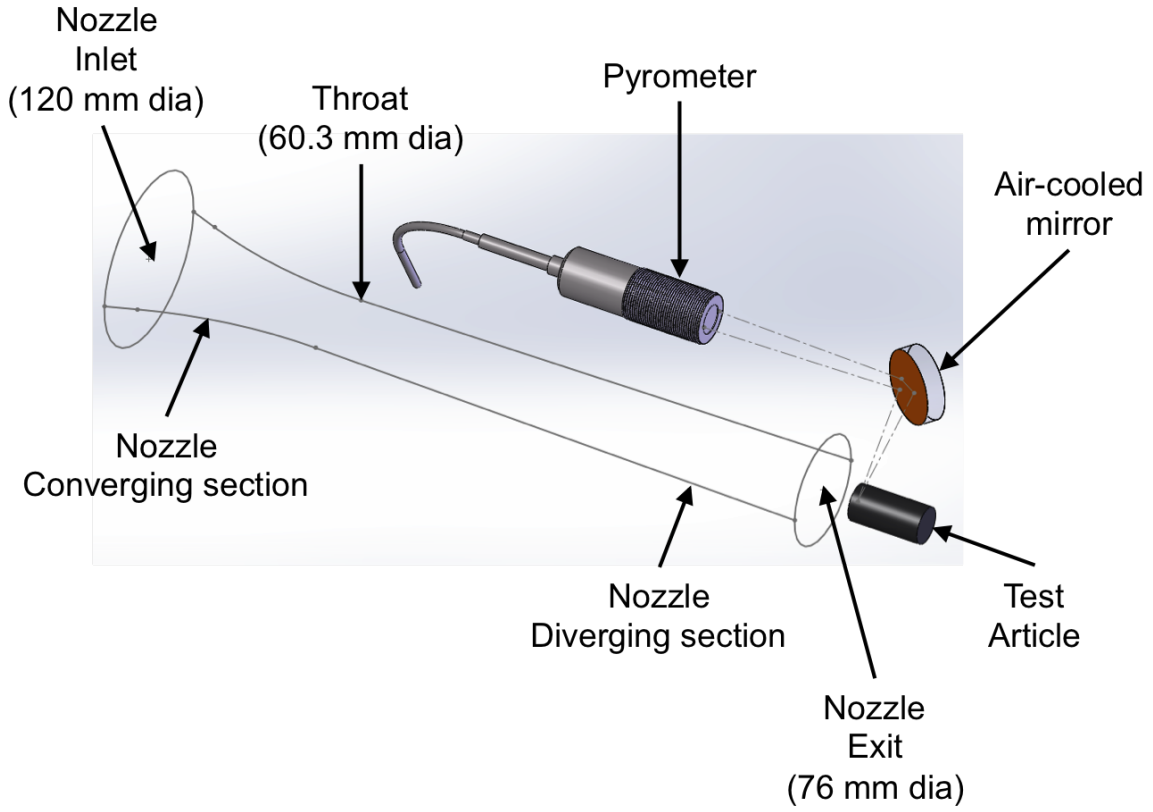

Figure 5: A wire frame outline of the inside nozzle contour (flow is from left to right), and the lens assembly of a fiber optic pyrometer, a gold faced mirror and a test sample. The wireframe geometry is used in flow field simulations.

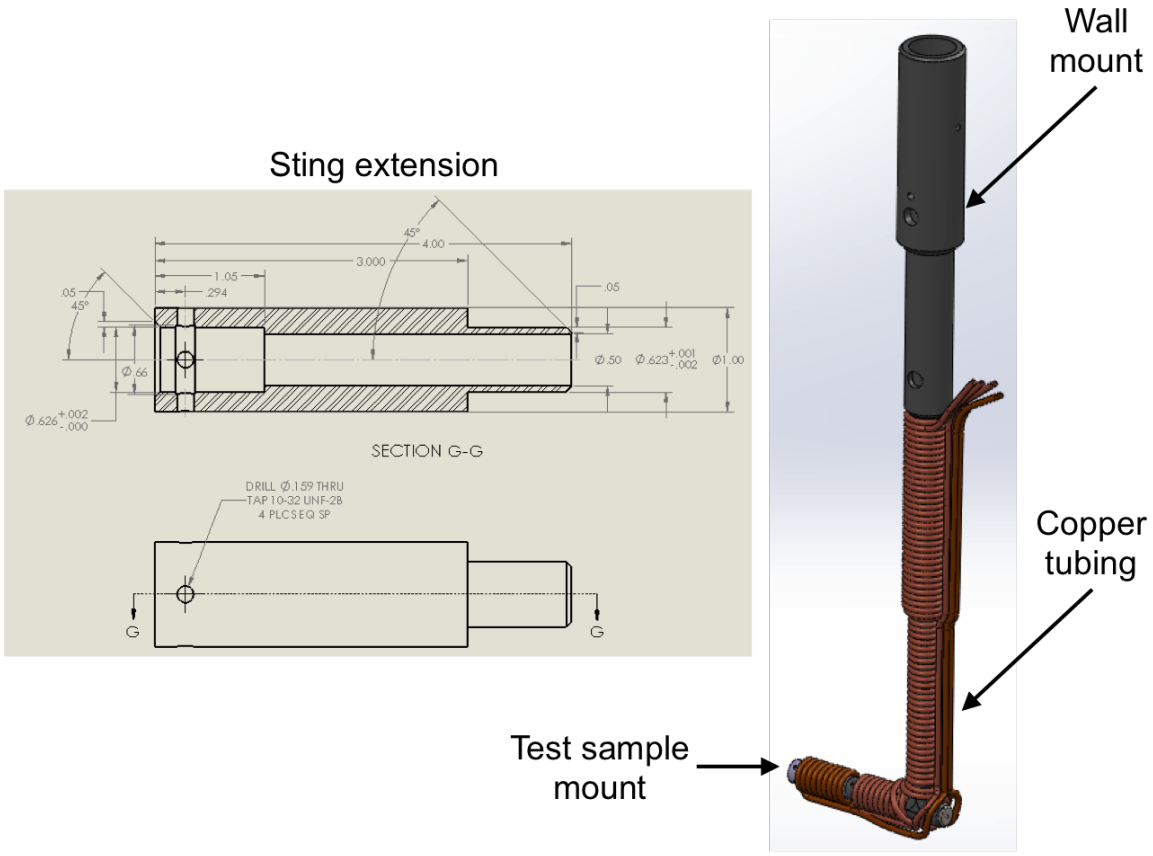

Figure 6: CAD model of sting. Test samples are mounted to the end of a welded tubular steel sting. The sting is thermally protected with a wrapping of thin-walled copper tube (6 mm or $\frac{1}{4}$ inch OD) circulating high pressure water. The sting extension for test samples has a 16 mm (dia) $\times$ 27 mm cavity. Instrumentation wiring must fit through the 13 mm (dia) passage.

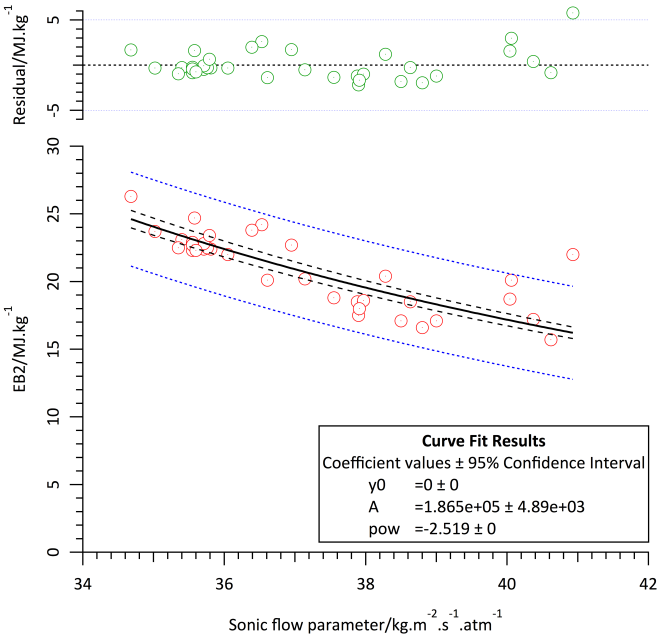

(a) Winovich fit

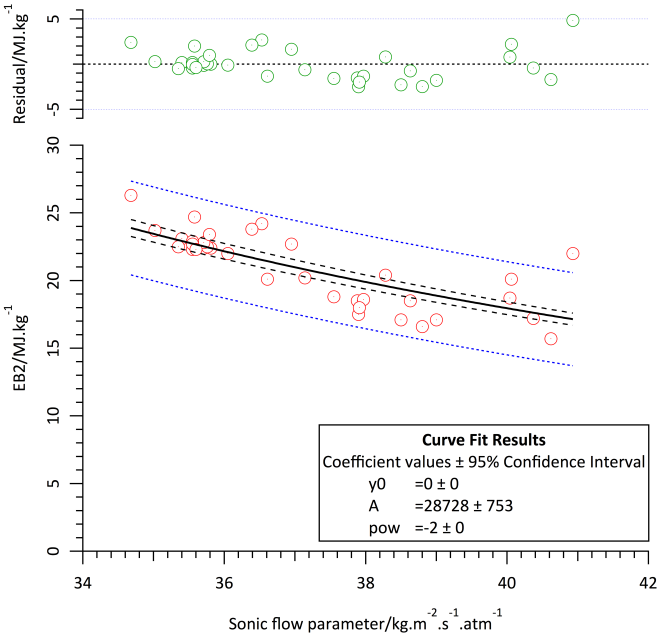

(b) Thompson *et al.* fit

Figure 7: Bulk enthalpy measurements (EB2) and power law fits to the data with sonic flow parameter, σ, as the independent variable (see Eq. 5). Data are from bulk enthalpy measurements made for heater settings used in the characterization of the 76 mm nozzle only (see Table 1).

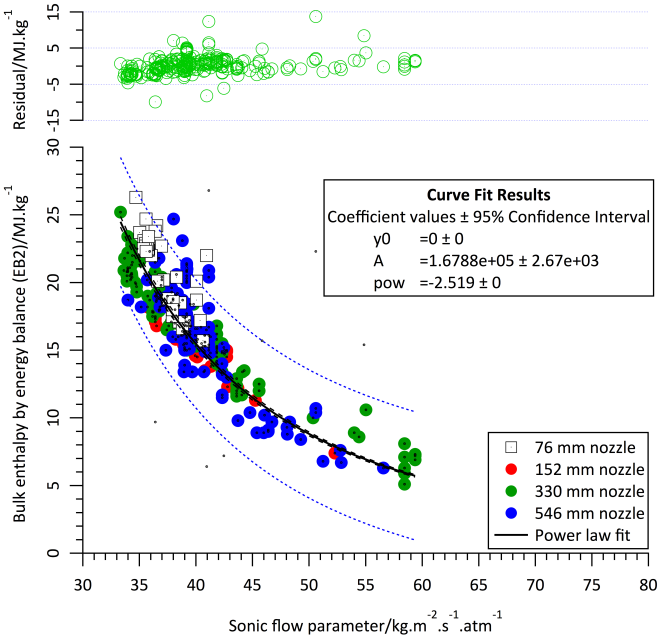

(a) Winovich fit

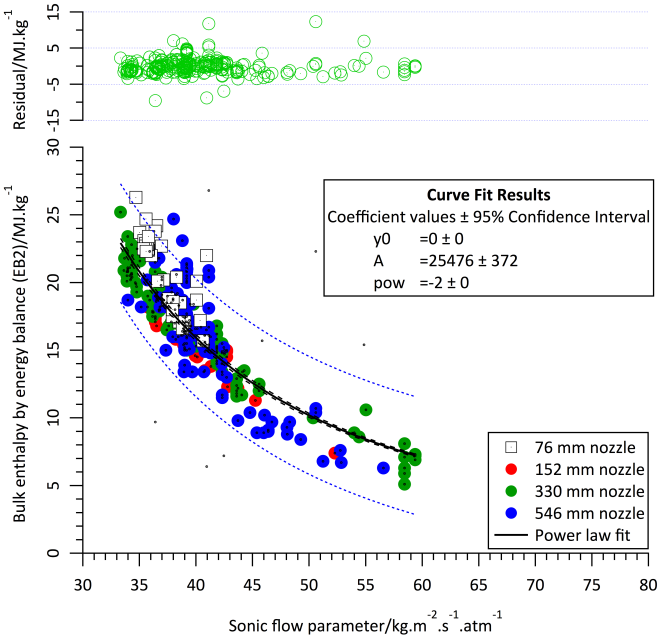

(b) Thompson *et al.* fit

Figure 8: Bulk enthalpy measurements (EB2) and power law fits to the data with sonic flow parameter, σ, as the independent variable (see Eq. 5). Historical data from bulk enthalpy measurements made for heater settings used in tests of other nozzles (152, 546, and 760 mm exit diameters) of the IHF are shown as closed symbols.

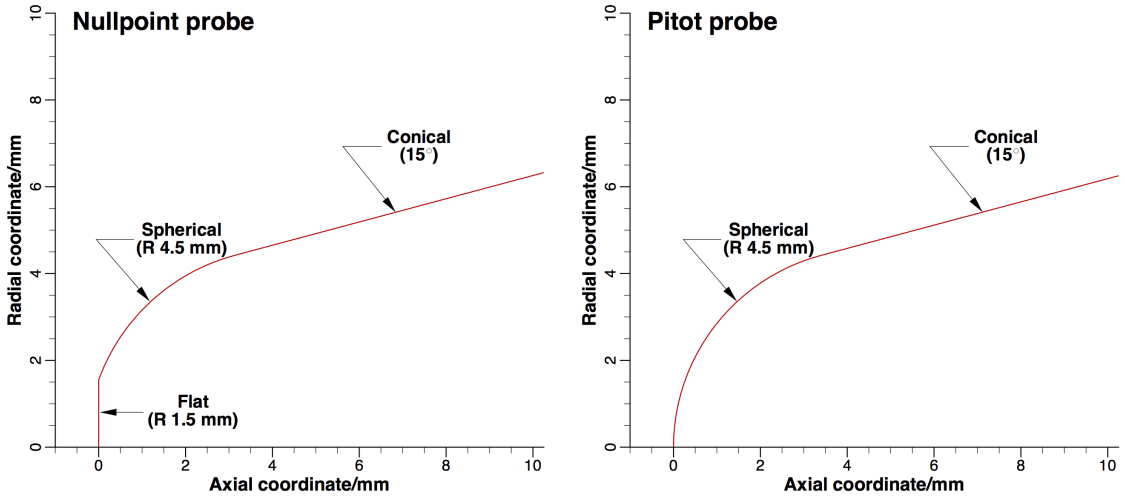

Figure 9: Heat flux and pressure probes used in the first round of characterization of the new 76 mm (3 inch) nozzle of the IHF.

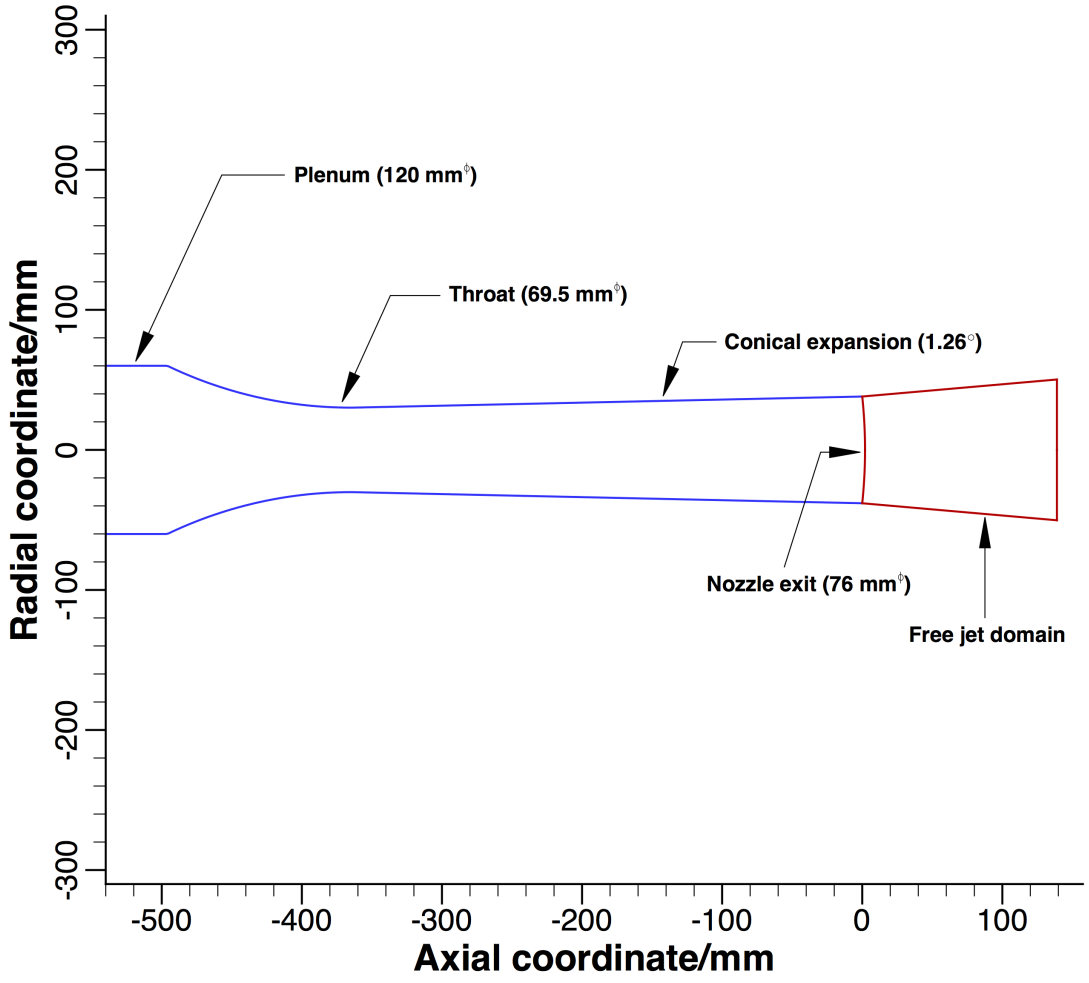

Figure 10: Geometry of the new 76 mm nozzle of the IHF at NASA Ames Research Center.

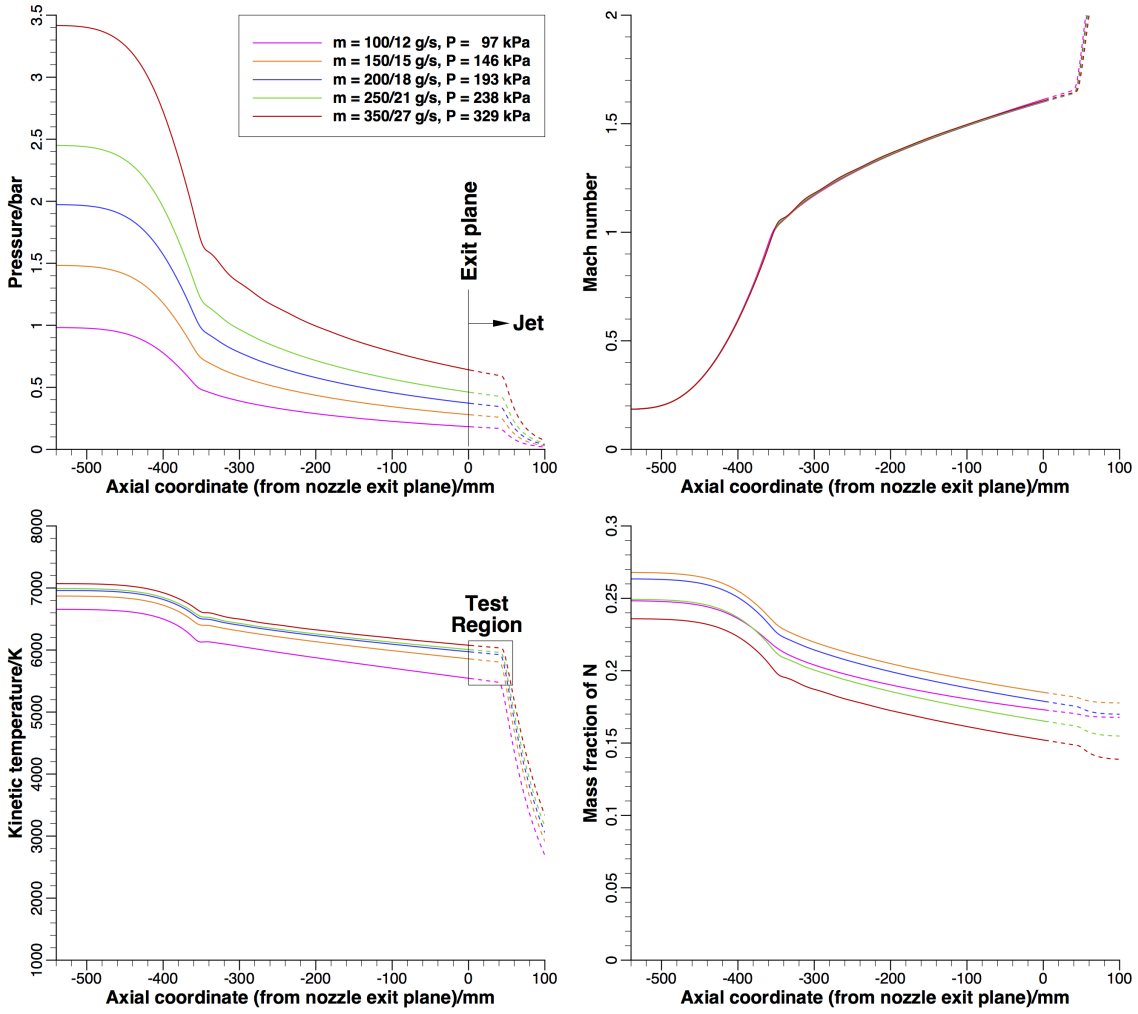

Figure 11: Centerline distributions of pressure, frozen Mach number, kinetic temperature, and mass fraction of N for an arc current of 2000 A and various arc column pressures.

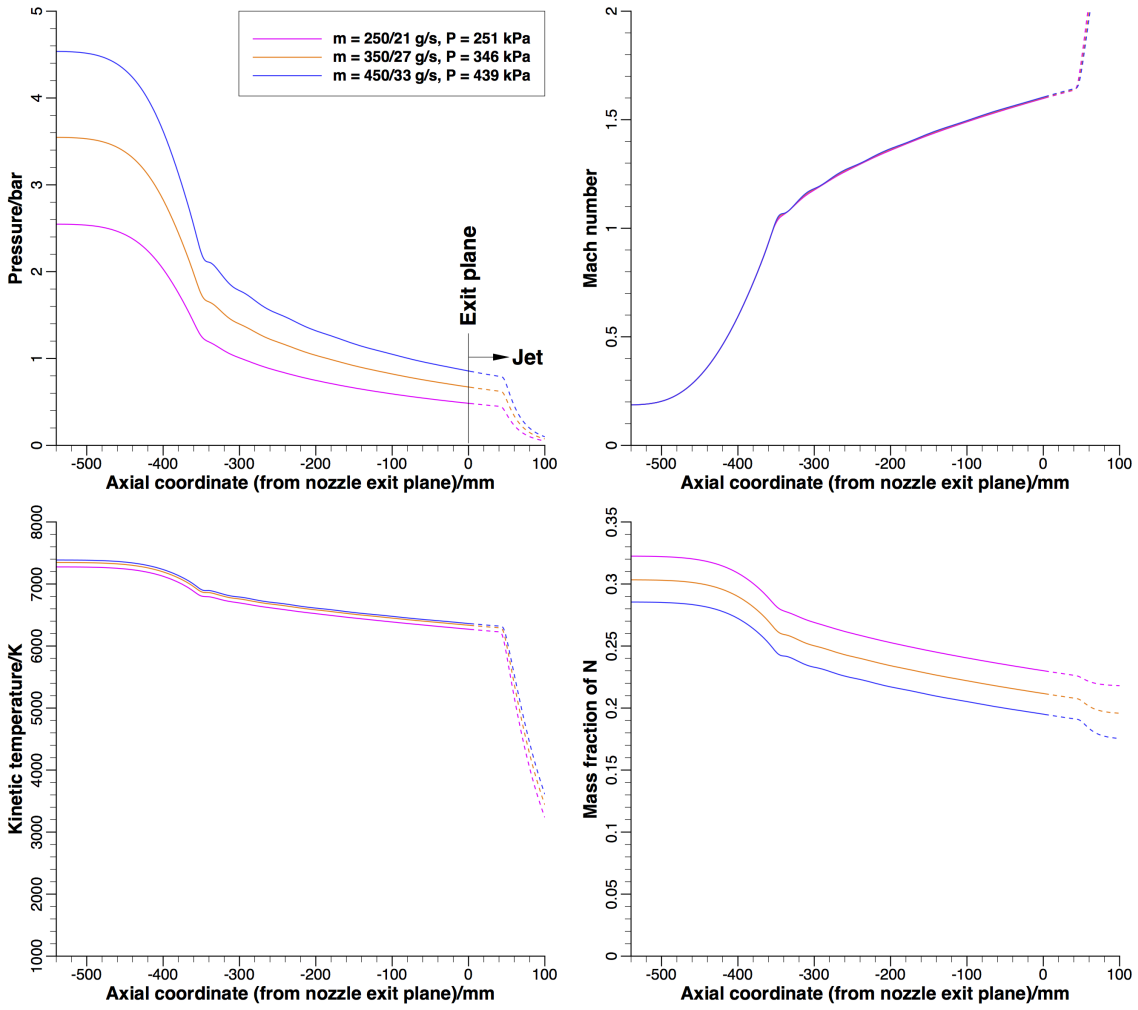

Figure 12: Centerline distributions of pressure, frozen Mach number, kinetic temperature, and mass fraction of N for an arc current of 3000 A and various arc column pressures.

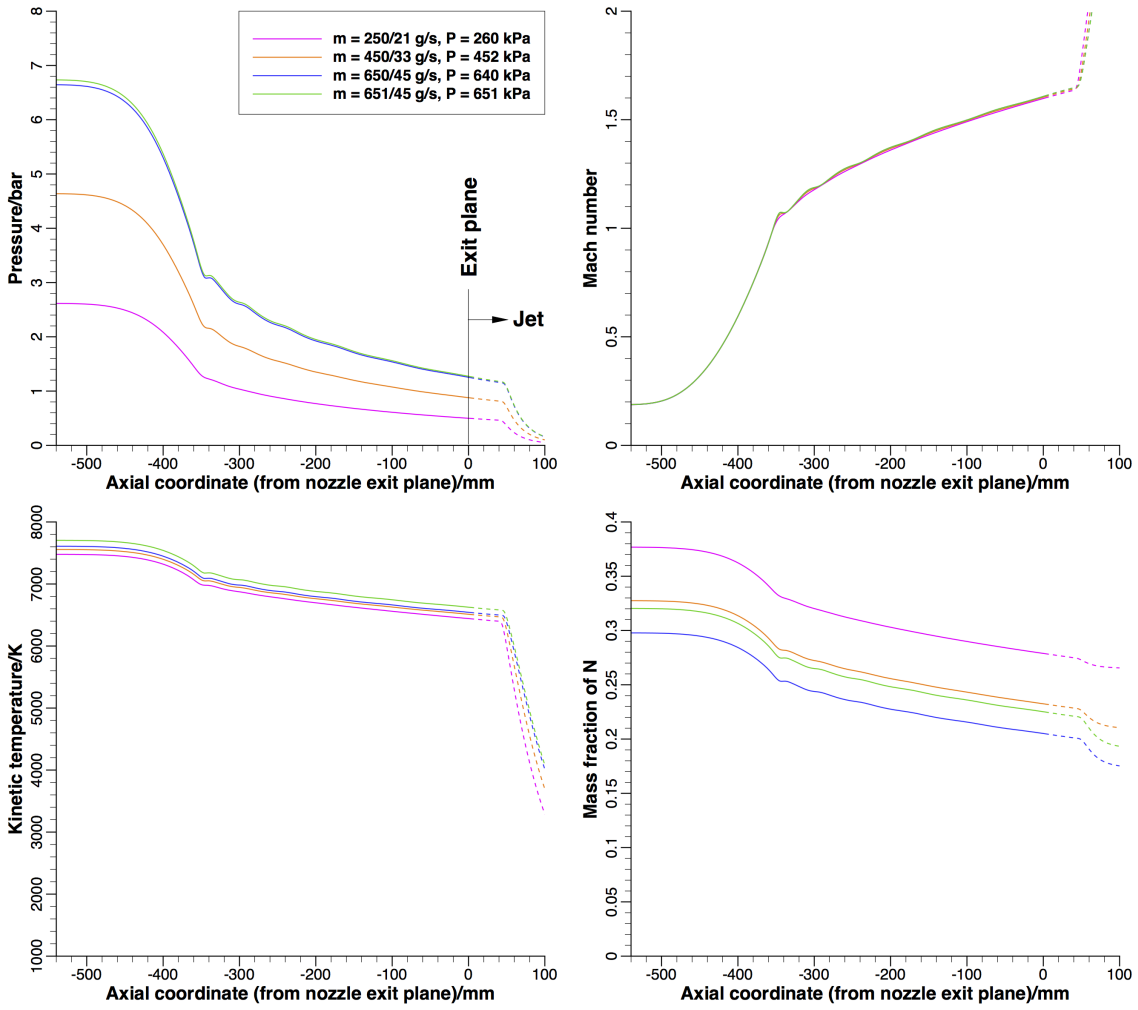

Figure 13: Centerline distributions of pressure, frozen Mach number, kinetic temperature, and mass fraction of N for an arc current of 3500 A and various arc column pressures.

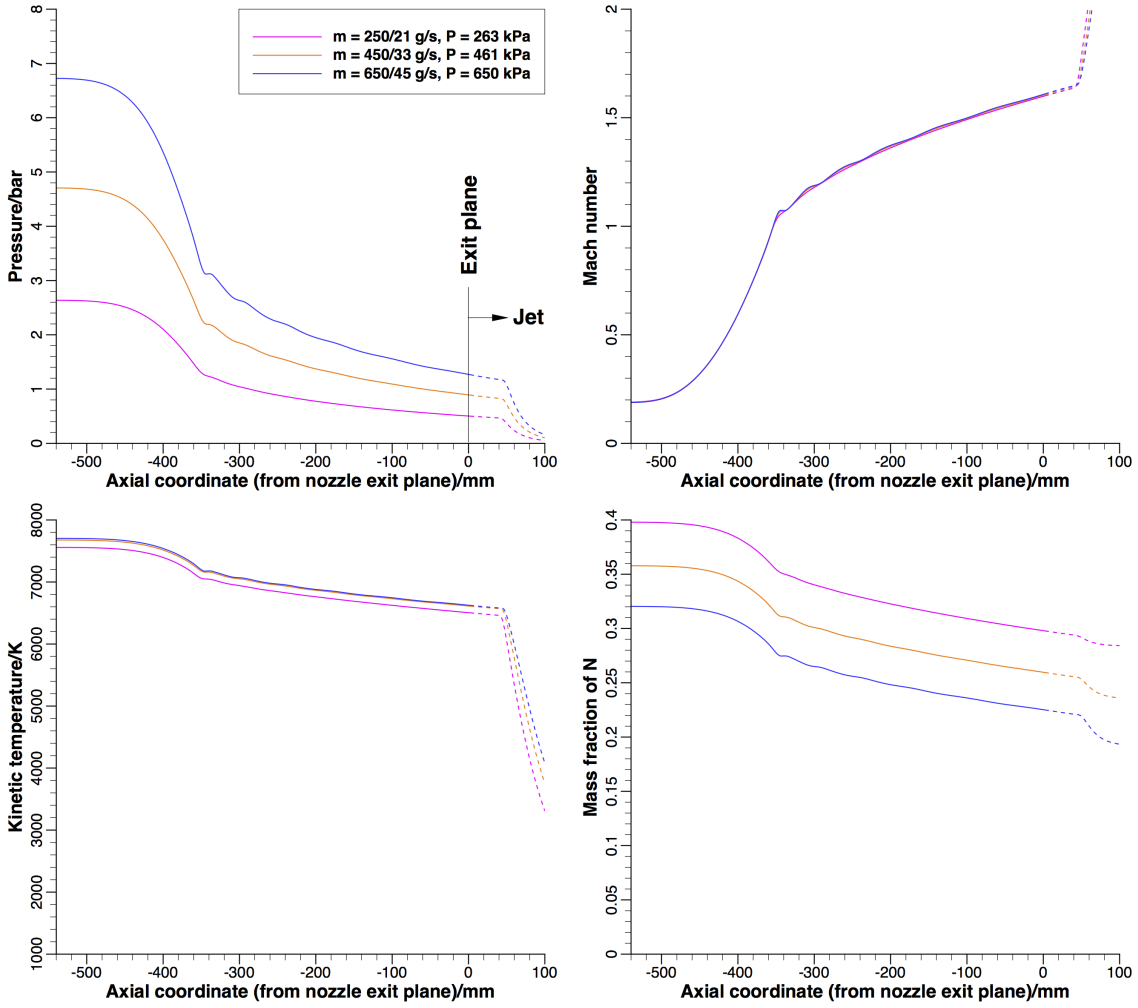

Figure 14: Centerline distributions of pressure, frozen Mach number, kinetic temperature, and mass fraction of N for an arc current of 4000 A and various arc column pressures.

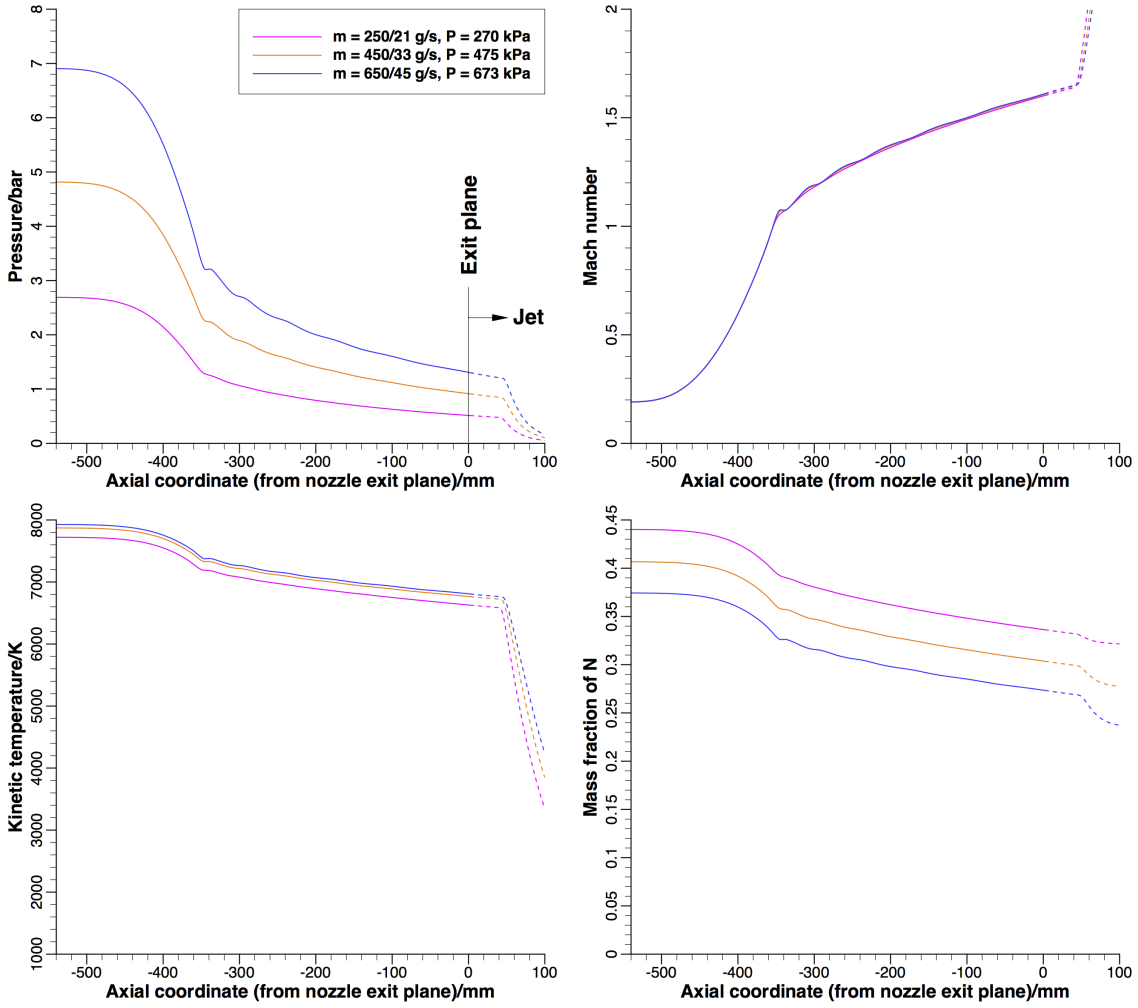

Figure 15: Centerline distributions of pressure, frozen Mach number, kinetic temperature, and mass fraction of N for an arc current of 5000 A and various arc column pressures.

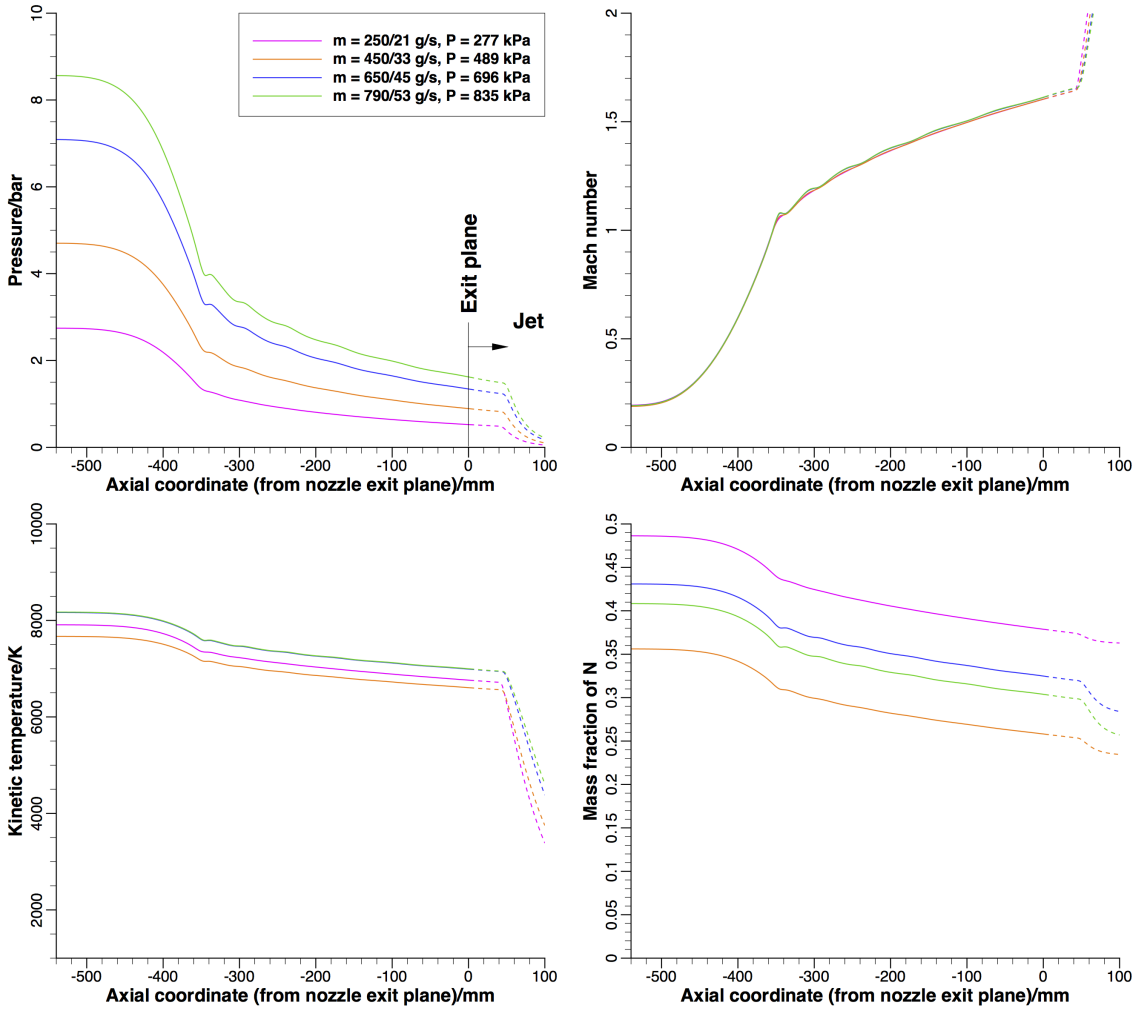

Figure 16: Centerline distributions of pressure, frozen Mach number, kinetic temperature, and mass fraction of N for an arc current of 6000 A and various arc column pressures.

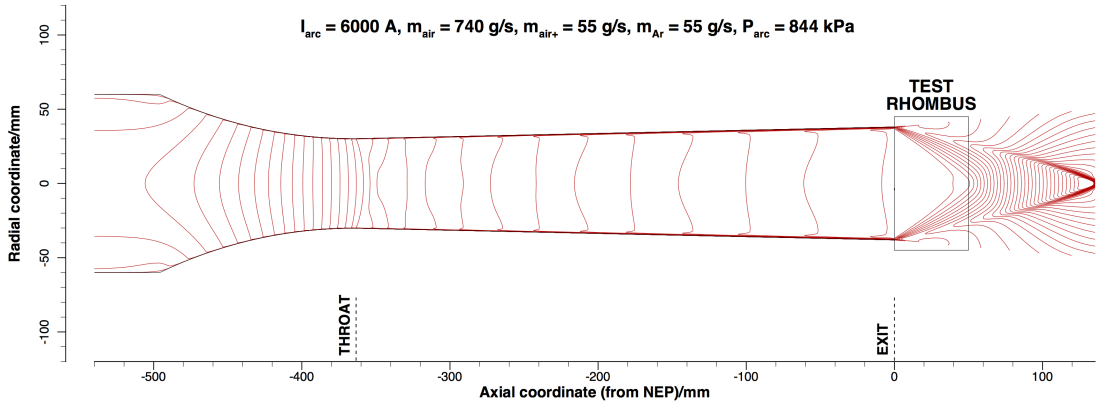

Figure 17: Pitch plane contours of frozen Mach number show the first "test rhombus" available. As should be expected, the test rhombus is small. The rhombus closes at roughly 50 mm (2 inches) from the nozzle exit plane (NEP).

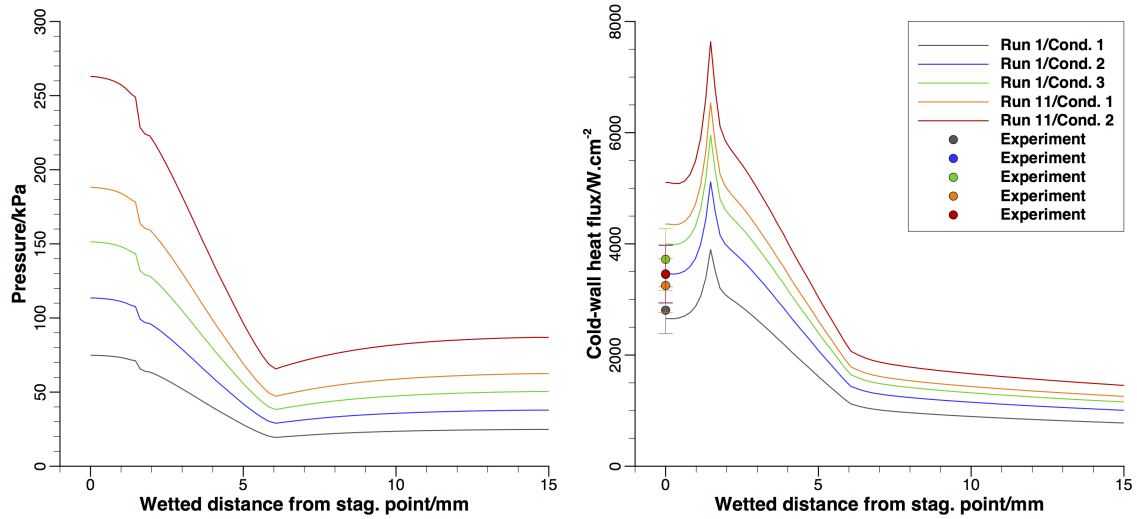

Figure 18: Distributions of surface pressure and heat flux over the nullpoint calorimeter geometry for an arc current of 2000 A and various arc column pressures. The symbols are nullpoint measurements.

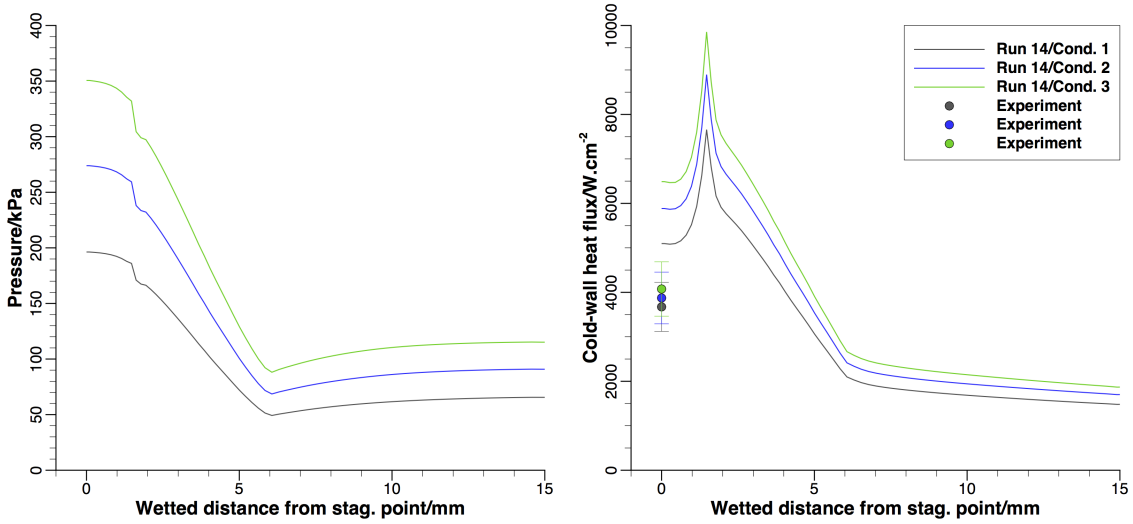

Figure 19: Distributions of surface pressure and heat flux over the nullpoint calorimeter geometry for an arc current of 3000 A and various arc column pressures. The symbols are nullpoint measurements.

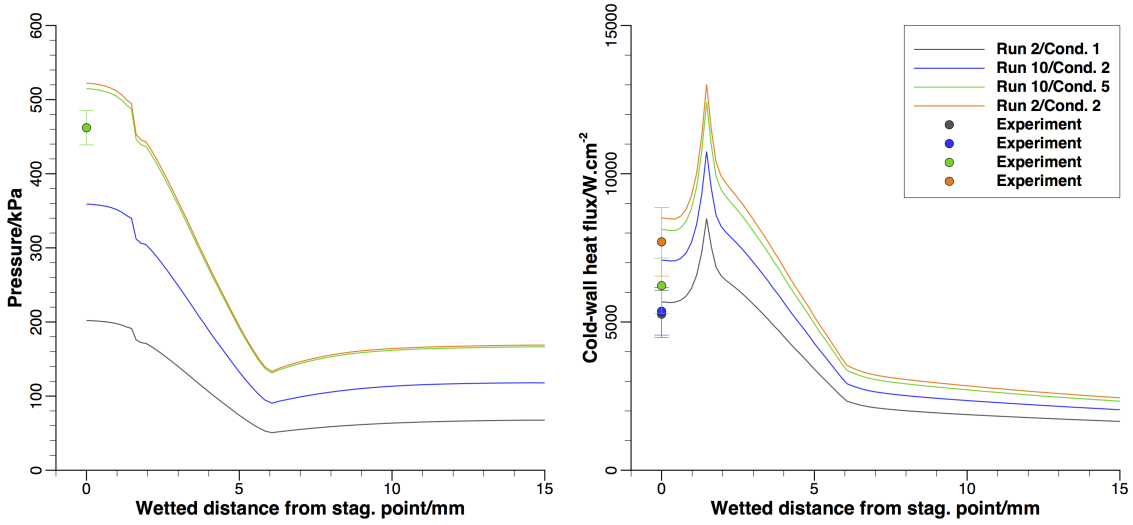

Figure 20: Distributions of surface pressure and heat flux over the nullpoint calorimeter geometry for an arc current of 3500 A and various arc column pressures. The symbols are nullpoint measurements. The only other successful pressure measurement at the highest arc column pressure of 640 kPa is also shown. The arc column pressure for the two cases, Run 10/Cond.5 and Run 2/Cond.2, are different – 640 kPa for the former, and 651 kPa for the latter.

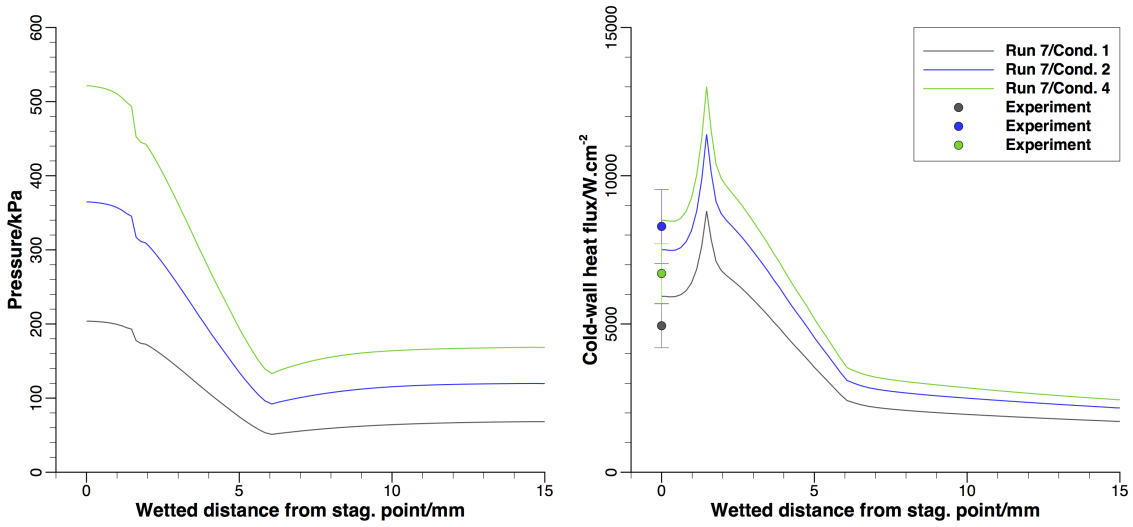

Figure 21: Distributions of surface pressure and heat flux over the nullpoint calorimeter geometry for an arc current of 4000 A and various arc column pressures. The symbols are nullpoint measurements.

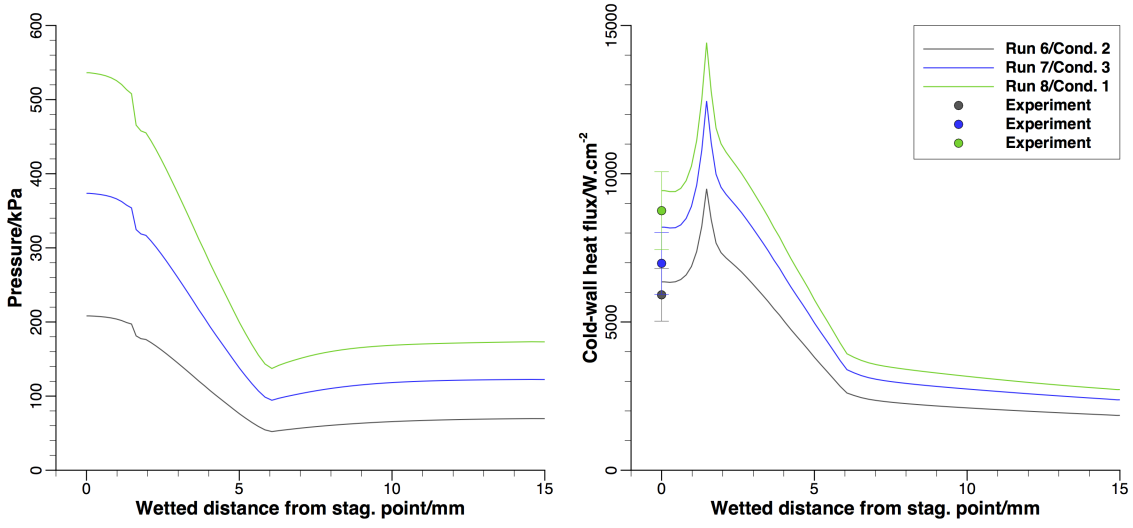

Figure 22: Distributions of surface pressure and heat flux over the nullpoint calorimeter geometry for an arc current of 5000 A and various arc column pressures. The symbols are nullpoint measurements.

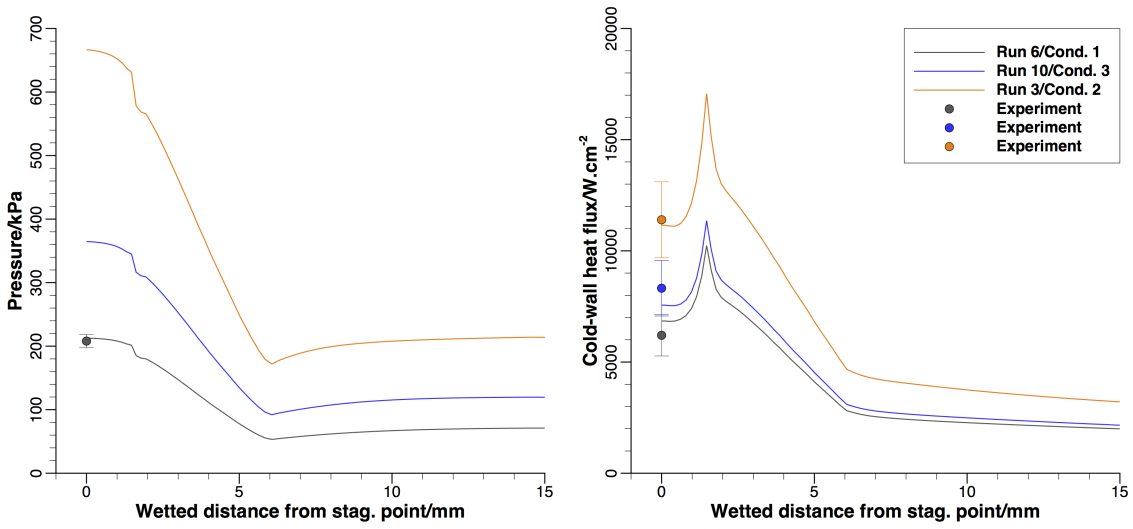

Figure 23: Distributions of surface pressure and heat flux over the nullpoint calorimeter geometry for an arc current of 6000 A and various arc column pressures. The symbols are nullpoint measurements. The only other successful pressure measurement at the lowest arc column pressure of 277 kPa is also shown.

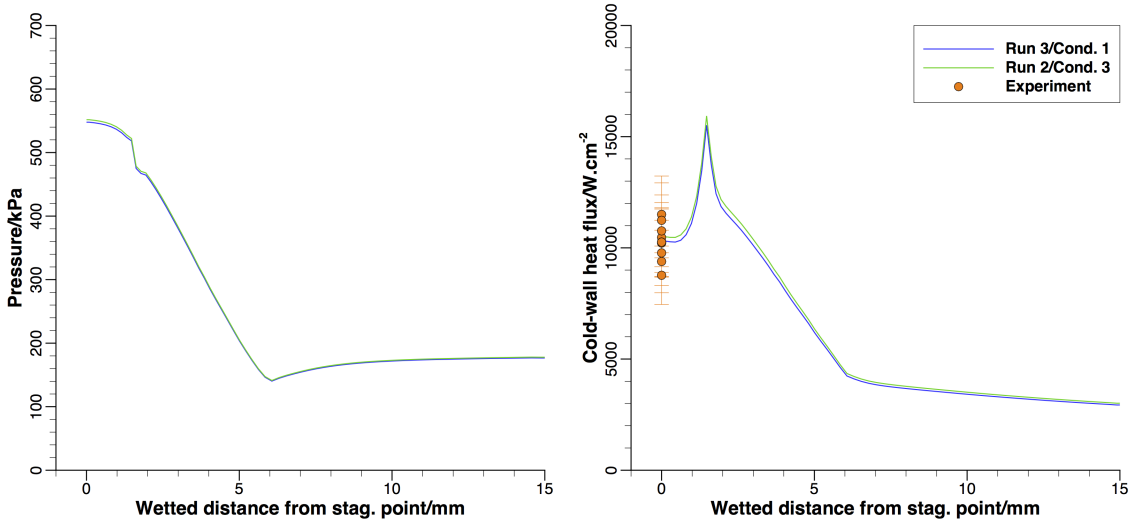

Figure 24: Distributions of surface pressure and heat flux over the nullpoint calorimeter geometry for an arc current of 6000 A and a flow rate of 650 g/s (air) and 45 g/s (Ar) for two arc column pressures - 690 and 696 kPa. The symbols are nullpoint measurements, which show ±15% scatter about their average value.

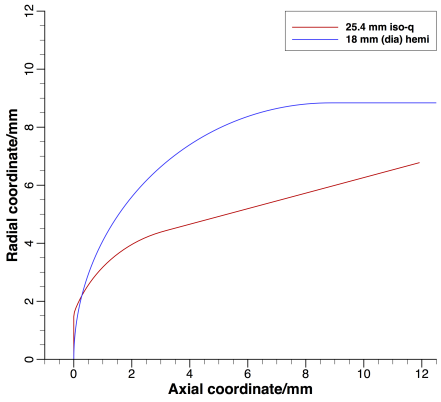

Figure 25: Comparison of the geometry of the nullpoint calorimeter and an equivalent hemisphere cylinder. The radius of the hemispherical cap is the "effective" radius of the nullpoint calorimeter.

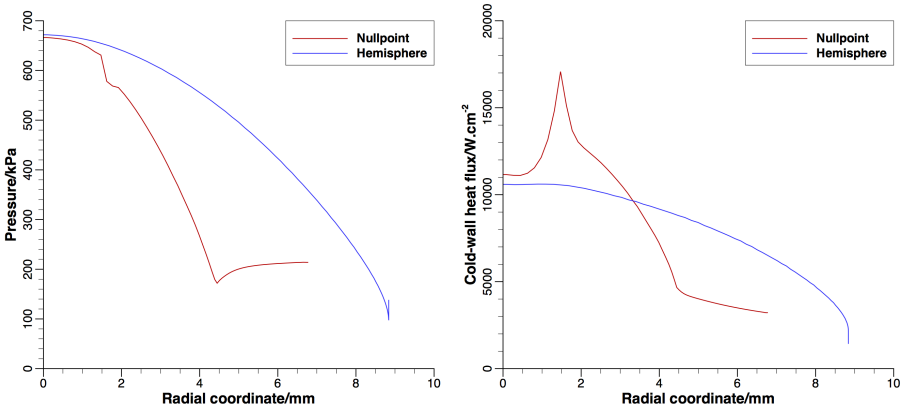

Figure 26: Comparison of the predicted surface pressure and cold-wall heat flux distributions for the nullpoint geometry and equivalent hemisphere cylinder. At the stagnation points of the two geometries, the predicted pressures and heat fluxes are within 5% of each other. Results are shown for Run #3/Condition #2 of the test matrix.

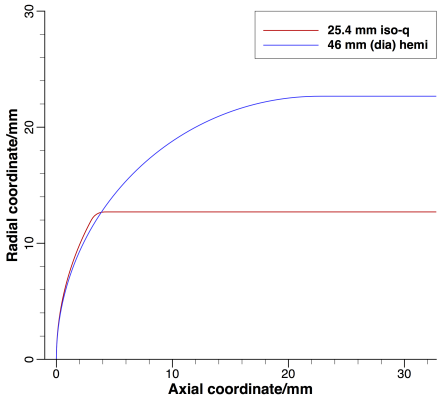

Figure 27: Comparison of the geometry of the iso-q and an equivalent hemisphere cylinder. The radius of the hemispherical cap is the "effective" radius of the iso-q geometry.

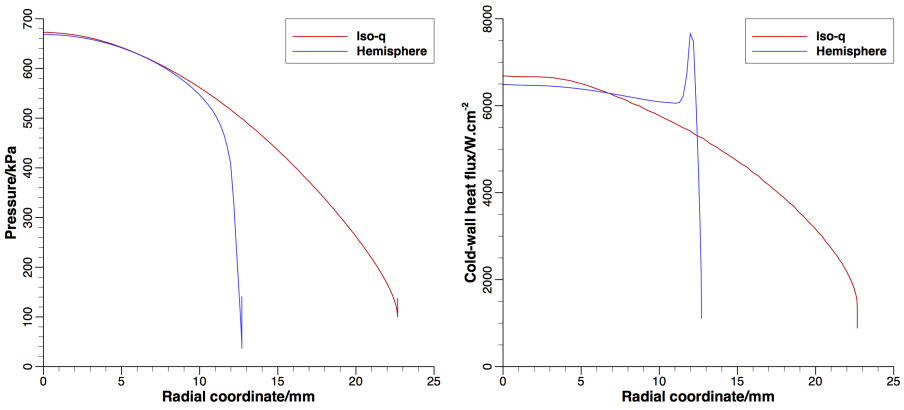

Figure 28: Comparison of the predicted surface pressure and cold-wall heat flux distributions for the nullpoint geometry and equivalent hemisphere cylinder. At the stagnation points of the two geometries, the predicted pressures and heat fluxes are within 3% of each other. Results are shown for Run #3/Condition #2 of the test matrix.

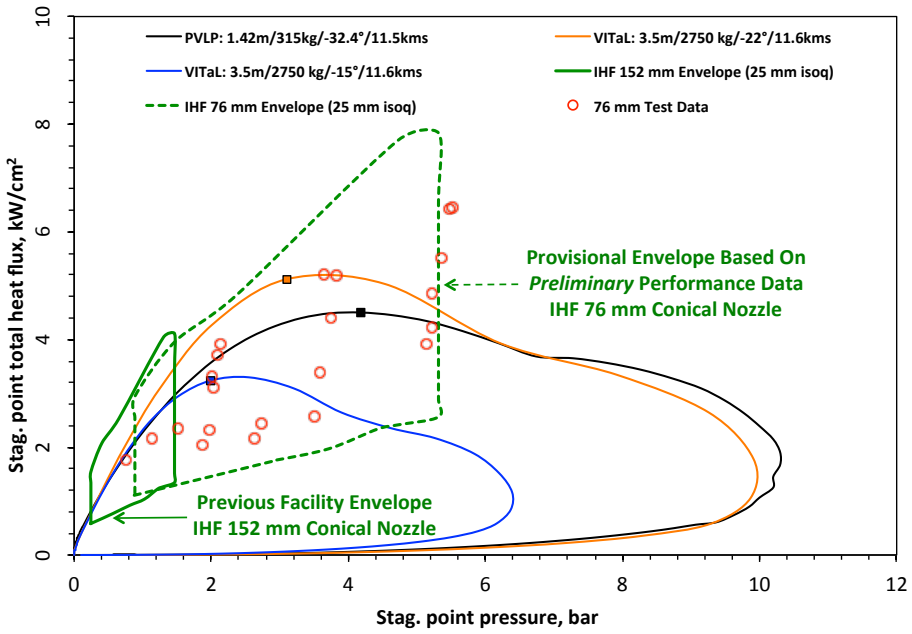

(a) Venus trajectories

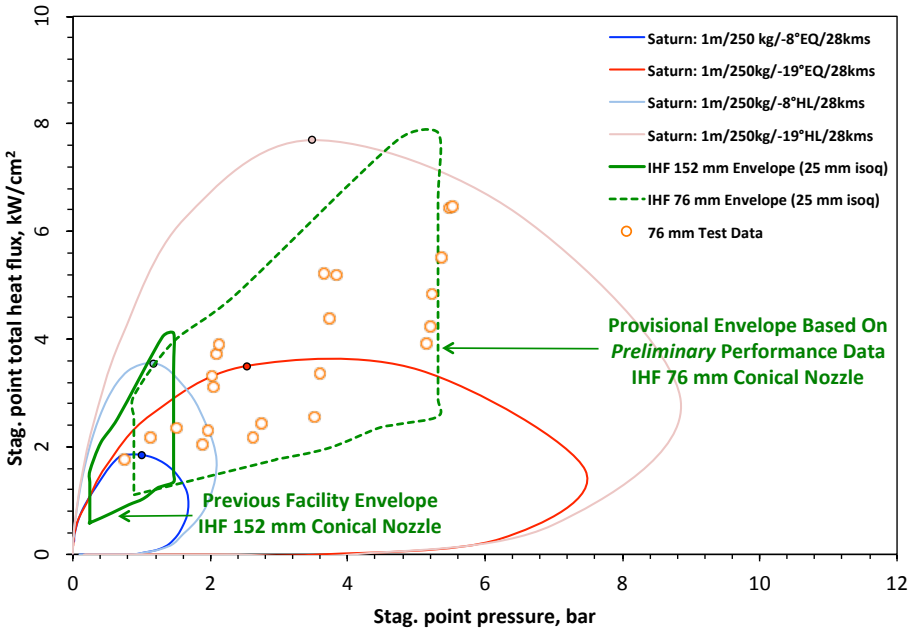

(b) Saturn trajectories

Figure 29: Provisional operating envelope (stag. point heat flux *vs.* pressure) of the new 76 mm nozzle of the IHF is shown with dashed boundary. The open symbols represent *measured* heat fluxes and *predicted* pressures. The operating envelope of the 152 mm nozzle is also shown, along with representative trajectory environments for Venus and Saturn atmospheric entries. The closed symbols shown indicate the points of peak heating along the trajectories. PVLP: *P*ioneer-*V*enus *L*arge *P*robe, and VITaL: *V*enus *I*ntrepid *T*essera *L*ander.

REPORT DOCUMENTATION PAGE

Form Approved
OMB No. 0704–0188

1. REPORT DATE *(DD-MM-YYYY)*	2. REPORT TYPE	3. DATES COVERED *(From - To)*
01-11-2015	Technical Memorandum	

4. TITLE AND SUBTITLE
Design and characterization of a new nozzle in a NASA arc-jet

5a. CONTRACT NUMBER
NNA10DE12C, NNA15BB15C, NNA09DB39C

5b. GRANT NUMBER

5c. PROGRAM ELEMENT NUMBER

6. AUTHOR(S)
Dinesh K. Prabhu, Imelda Terrazas-Salinas, Eric A. Noyes, and John A. Balboni

5d. PROJECT NUMBER

5e. TASK NUMBER

5f. WORK UNIT NUMBER

7. PERFORMING ORGANIZATION NAME(S) AND ADDRESS(ES)
NASA Ames Research Center
Moffett Field, California 94035

8. PERFORMING ORGANIZATION REPORT NUMBER
L–

9. SPONSORING/MONITORING AGENCY NAME(S) AND ADDRESS(ES)
National Aeronautics and Space Administration
Washington, DC 20546-0001

10. SPONSOR/MONITOR'S ACRONYM(S)
NASA

11. SPONSOR/MONITOR'S REPORT NUMBER(S)
NASA/TM–2015–218934

12. DISTRIBUTION/AVAILABILITY STATEMENT
Unclassified-Unlimited
Subject Category
Availability: NASA CASI (443) 757-5802

13. SUPPLEMENTARY NOTES
An electronic version can be found at http://ntrs.nasa.gov.

14. ABSTRACT

The design of a new 76 mm (3 inch) nozzle of the Interaction Heating Facility arc jet at NASA Ames Research Center is described. The computational efforts which were an integral part of the preliminary design and characterization of the nozzle are described as well. Details of heat flux measurements made in this new nozzle are provided. Apart from showing the flow characteristics of the nozzle, predictions of stagnation point heat flux are compared against measurements made with a nullpoint calorimeter; the agreement between computation and measurement is found to be good. Unfortunately, pressure measurements could not be made in the first round. Predicted stagnation point pressures and measured heat fluxes are used to establish a provisional operating envelope for the new nozzle. The envelope is shown to enclose relevant heating portions of representative atmospheric trajectories at Venus and Saturn.

15. SUBJECT TERMS
Arc-jet, nozzle deisgn, numerical simulation, calorimetry, operational envelope

16. SECURITY CLASSIFICATION OF:			17. LIMITATION OF ABSTRACT	18. NUMBER OF PAGES	19a. NAME OF RESPONSIBLE PERSON
a. REPORT	b. ABSTRACT	c. THIS PAGE			STI Information Desk (help@sti.nasa.gov)
U	U	U	UU		19b. TELEPHONE NUMBER *(Include area code)* (443) 757-5802